Status of thesis

Title of thesis | Development of Cu/TiO_2 Photocatalyst for Hydrogen Production under Visible Light

I LEONG SIEW YOONG

hereby allow my thesis to be placed at the Information Resource Center (IRC) of Universiti Teknologi PETRONAS (UTP) with the following conditions:

1. The thesis becomes the properties of UTP.
2. The IRC of UTP may make copies of the thesis for academic purposes only.
3. This thesis is classified as

☐ Confidential

☑ Non-confidential

If this thesis is confidential, please state the reason:

-

The contents of the thesis will remain confidential for - years.

Remarks on disclosure:

-

Endorsed by

Signature of Author

7, Persiaran Zarib 5,
Taman Pinji Mewah,
31500, Lahat, Perak

Date : 28/5/09

Signature of Supervisor

DR CHONG FAI KAIT
Sr. Lecturer
Fundamental & Applied Sciences Department
Universiti Teknologi PETRONAS PERAK

Department of Chemical Engineering
Universiti Teknologi PETRONAS
Perak

Date : 28/5/09

UNIVERSITI TEKNOLOGI PETRONAS

Approval by Supervisor (s)

The undersigned certify that they have read, and recommend to The Postgraduate Studies Programme for acceptance, a thesis entitled **"Development of Cu/TiO_2 Photocatalyst for Hydrogen Production under Visible Light"** submitted by **(Leong Siew Yoong)** for the fulfillment of the requirements for the degree of Master of Science in Chemical Engineering.

28/5/09

Date

Signature :

Main supervisor :

DR CHONG FAI KAIT
Senior Lecturer
Fundamental & Applied Sciences Department
Universiti Teknologi PETRONAS, PERAK

Date : 28/5/09

UNIVERSITI TEKNOLOGI PETRONAS

Development of Cu/TiO_2 Photocatalyst for Hydrogen Production under Visible Light

By

Leong Siew Yoong

A THESIS

SUBMITTED TO THE POSTGRADUATE STUDIES PROGRAMME

AS A REQUIREMENT FOR THE

DEGREE OF MASTER OF SCIENCE

CHEMICAL ENGINEERING

BANDAR SERI ISKANDAR,

PERAK

MAY, 2009

I hereby declare that the thesis is based on my original work except for quotations and citations which have been duly acknowledged. I also declare that it has not been previously or concurrently submitted for any other degree at UTP or other institutions.

Signature : 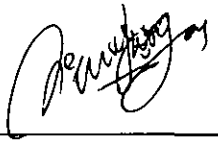

Name : LEONG SIEW YOONG

Date : 28/5/09

Acknowledgement

This dissertation was made possible by the help and support of many people. First of all, I would like to express my sincere gratitude and appreciation to my supervisor, Dr. Chong Fai Kait, for providing me with this unique research opportunity, and for her guidance and support all the way in my two years period of study and preparation of this thesis. Throughout my study and research project, she has constantly given me insightful advice. I have not only learnt from her but have also been inspired by her dedicated attitude to science. It has been a marvelous learning experience.

I would like to acknowledge all the staff members in the Chemical and Mechanical Engineering Department for their contributions to an active academic atmosphere. In addition, this research work was made possible by the generous financial support from the MOSTI (E-Science grant 03-02-02-SF0002).

Lastly, and most importantly, I felt very grateful to my parents for their unending support and love for the pursuit of my MSc. Thank you always for being there to support me.

ABSTRACT

Technologies for generating hydrogen from water using modified photocatalyst have drawn many attentions. In this study the photocatalysts for hydrogen generation were synthesized using two methods; complex-precipitation and wet impregnation method. Cu/TiO_2 with 2, 5, 10 and 15 wt% loading was prepared, dried and prior to calcination, thermal gravimetric analysis was carried out to determine their thermal stability. Based on the thermograms, the calcination temperature was estimated to be 300°C or higher. Therefore, the photocatalysts were calcined at 300°C, 400°C and 500°C for 30 min. The effect of transition metal loading and calcination temperatures on the photocatalytic activity was investigated. Photocatalytic activity was carried out under visible light illumination (500 W halogen lamp as the light source). The screening process is used to monitor the photocatalytic activities for hydrogen production in a multiport reactor containing of photocatalyst, water and methanol (as scavenger). For all photocatalysts, the highest amount of hydrogen produced was 8.5 $mLg^{-1}h^{-1}$ for Cu/TiO_2 calcined at 300°C C for 30 min prepared using complex-precipitation method. The amount of hydrogen produced decrease as the calcination temperature increases for all the catalysts. The photocatalysts were also characterized using Temperature Programmed Reduction (TPR), Diffuse Reflectance UV-Vis (DR-UV-Vis), Field Emission Scanning Electron Microscope (FE-SEM), Fourier Transform Infared (FTIR), X-ray Difractometer (XRD) and surface area determination (BET). The results from TPR and XRD indicated that the only Cu species present was CuO supported on TiO_2. The SEM micrographs showed morphology of the prepared samples with particle size around 20 nm to 100 nm. The effect of transition metal loading was studied and found that incorporating with copper enhance the photocatalytic activity compared to TiO_2. However higher concentration of transition metal loading up to 15 wt% led to the decrement of the photocatalytic activity. The lower photocatalytic activity can be influence by the surface saturation of Cu which minimized the light penetration from reaching to the surface of the TiO_2. The incorporation of Cu transition metal had successfully shifted the TiO_2 band gap to a longer wavelength as evidence by DR-UV-Vis.

ABSTRAK

Teknologi untuk penghasilan hidrogen dari air dengan menggunakan modifikasi fotomangkin telahpun mendapat banyak perhatian. Fotomangkin Cu/TiO_2 yang telah disintesis menggunakan dua teknik iaitu pemendakan-kompleks dan impregnasi basah telah diaplikasikan dalam penyelidikan ini. Cu/TiO_2 dengan kandungan logam sebanyak 2, 5, 10 dan 15 wt% telah disediakan dan dikeringkan. Seterusnya, penentuan suhu penguraian menggunakan TGA yang dilakukan keatas fotomangkin segar sebelum meneruskan proses kalsinasi. Berdasarkan graf penguraian tersebut, suhu minimum bagi kalsinasi ialah 300°C dan ke atas. Seterusnya, fotomangkin dikalsin pada suhu 300°C, 400°C dan 500°C selama 30 min. Kegiatan fotoaktiviti untuk penghasilan hidrogen dijalankan di dalam multiport yang berisi fotomangkin, air dan metanol (sebagai bahan korban) di bawah sinaran lampu halogen 500 W sebagai sumber cahaya untuk semua fotomangkin. Kegiatan fotoaktiviti juga dijalankan tanpa menggunakan metanol sebagai eksperiment terkawal. Berdasarkan keputusan dari pengskrinan, fotoaktiviti optimum adalah bagi fotomangkin 10 wt% bagi kedua-dua kaedah. Pencirian fotomangkin Cu/TiO_2 ini telah dilakukan dengan menggunakan Penurunan Berprogramkan Suhu (TPR), Membaur Refleksi UV-Vis (DR-UV-Vis), Bidang Emisi Pengimbasan Elektron Mikroskop (FE-SEM), Fourier Transformasi Inframerah (FTIR), Pembelauan Sinar-X (XRD), teknik penjerapan fizik (BET) dan Analisa Terma Gravimetrik (TGA). Kesan penambahan kandungan Cu dan peningkatan suhu kalsinasi ke atas kegiatan fotoaktiviti tersebut disiasat. Jumlah penghasilan hidrogen yang tertinggi ialah 8.5 $mLg^{-1}h^{-1}$ bagi Cu/TiO_2 yang disediakan menggunakan kaedah pemendakan-komplex dan dikalsinasi pada suhu 300°C selama 30 min. Fotoaktiviti penghasilan hidrogen bagi semua fotomangkin didapati menurun apabila suhu kalsinasi meningkat. Keputusan XRD yang diperolehi menunjukkan kehadiran spesis CuO sahaja. FE-SEM menunjukkan bahawa morfologi untuk butiran sampel adalah dalam julat sekitar 20 nm ke 100 nm. Kesan daripada penambahan Cu yang dikaji dan didapati bahawa aktiviti fotomangkin dipertingkatkan berbanding dengan TiO_2. Namun demikian, kandungan Cu yang berlebihan (15 wt%) mengakibatkan penurunan kegiatan fotomangkin. Penurunan fotoaktiviti disebabkan oleh kepekatan Cu yang terlalu tinggi dan seterusnya

mengurangkan penembusan cahaya untuk sampai ke permukaan TiO_2. Penambahan Cu dari unsur peralihan menyebabkan pengurangan "band gap" berbanding dengan TiO_2 (3.2 eV) sepertimana yang telah dibuktikan oleh DR-UV-Vis dan membolehkan fotomangkin yang telah dimodifikasi ini untuk menyerap lebih banyak cahaya tampak.

TABLE OF CONTENTS

LIST OF TABLES

LIST OF FIGURES

LIST OF SYMBOLS

W	-	Watt
$h\nu$	-	Photon energy
e^-	-	electron
h^+	-	hole

LIST OF ABBREVATIONS

TPR	-	Temperature Programmed Reduction
FTIR	-	Fourier Transform Infared
DR-UV-VIS	-	Diffuse Reflectance UV visible
FE-SEM	-	Field Emission Scanning Electron Microscope
XRD	-	X-ray Diffractometer
BET	-	Brunauer-Emmet-Teller
TGA	-	Thermal Gravimetric Analyzer
R&D	-	Research and Development
C.B	-	Conduction band
V.B	-	Valence band
SAA	-	Specific surface area
K	-	Kelvin
nm	-	nanometer
mA	-	mili Ampere
kV	-	kilo Volt
KM	-	Kubelka-Munk

CHAPTER 1

INTRODUCTION

1.1 Hydrogen Production

Hydrogen has been identified as a potential alternative fuel as well as an energy carrier for the future. Hydrogen is clean and can be produced from water which can be converted to energy in the form of electricity via fuel cell. Presently hydrogen is commonly produced from fossil fuels. Natural gas steam reforming is one of the economical hydrogen production processes. Only about 5% hydrogen is produced from renewable sources (Meng *et al.*, 2006; Momirlan and Veziroglu, 1999). Water electrolysis that can be driven by photovoltaic (PV) cells or wind turbines is an important hydrogen production process using renewable sources. Certain hydrogen production processes for instance, hydrogen production from steam reforming of natural gas, catalytic decomposition of natural gas, partial oxidation of heavy oils, coal gasification and steam-iron coal gasification have reached maturity for commercial exploitation. Other processes such as thermochemical, photochemical, photoelectrochemical and photobiological processes are being explored or already at the research and development stage. The main processes for hydrogen production and their status of development are summarized in Table 1.1. Solar hydrogen production technologies include solar thermochemical, photoelectrochemical, photocatalytic and photobiological hydrogen productions are also some of the promising sources for hydrogen production. In thermochemical hydrogen production, water is decomposed into hydrogen and oxygen through combinations of chemical reactions, and these reactions are carried out by utilizing only heat to drive them. When water and heat energy is given to the system, only the elemental constitute (H_2 and

O_2) and waste heat is generated. Photobiological system generally uses the natural photosynthetic activity of bacteria and green algae to produce H_2. This technology covers a vast range of approaches, including direct and indirect biophotolysis, photofermentation and dark-fermentation.

Table 1.1 Summary of main hydrogen production process (Momirlan and Veziroglu, 1999).

Production process	Status
Steam reforming of natural gas	Mature
Catalytic decomposition of natural gas	Mature
Partial oxidation of heavy oil	Mature
Coal gasification	R&D-mature
Steam-iron coal gasification	R&D
Water electrolysis	Mature
Thermochemical cycles (pure)	R&D
Thermochemical cycles (hybrid)	R&D
Photochemical processes	Early R&D
Photoelectrochmical processes	Early R&D
Photobiological processes	Early R&D

Photochemical and photoelectrochemical hydrogen production using solar energy are quite similar to the thermochemical system where it employs a system consisting chemical reactants in water splitting. Nevertheless, the driving force is not thermal energy but light. The mechanisms happened when a semiconductor was irradiated by photons (light) having energy equal to or greater than the band gap energy, where electrons are promoted from the valence band to the conduction band leaving positively charged hole in the valence band (Figure 1.1). If the conduction band edge is more negative than the hydrogen production level and the valance band is more positive than the oxygen production level, the photo-generated electron/hole pairs are able to decompose water into H_2 and O_2 (Agus *et al.*, 2005; Meng *et al.*, 2006). However with the present development, the hydrogen production rate is still low mainly due to a few factors: - the

quick electron/hole recombination in the bulk or on the surface of semiconductor particles, fast backward reaction of oxygen and hydrogen to form water on the surface of the catalyst and the inability to utilize visible light. Addition of electron donors (as hole scavengers) and incorporation of metal loading can enhance hydrogen production significantly due to reduction in charge recombination. The photochemical and photoelectrochemical hydrogen production is currently under active R&D but in future it will play a significant role in the hydrogen economy.

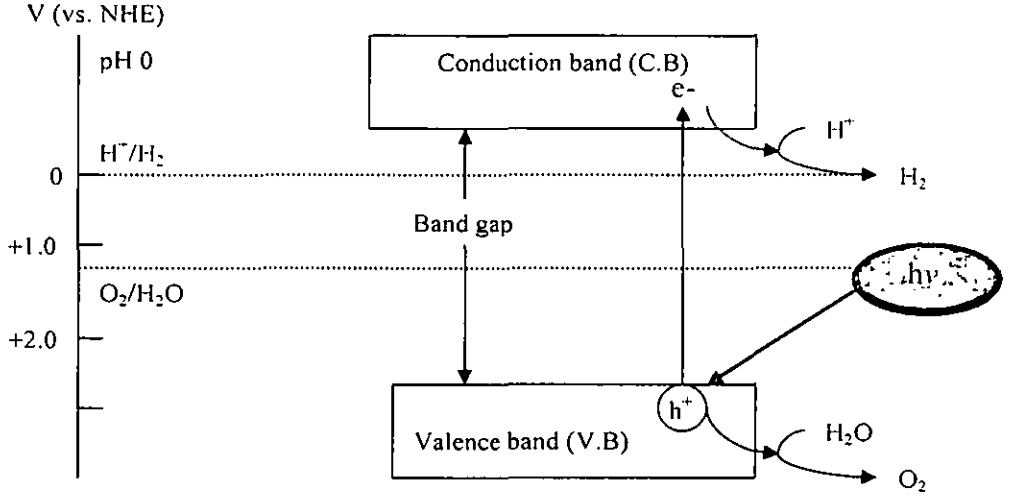

Figure 1.1 Basic principle of overall water splitting on a photocatalyst (Kazuhiko and Kazunari, 2007).

Hydrogen obtained from solar energy (solar hydrogen) combines the advantages of hydrocarbons (storability and transportability) with the advantages of solar energy (ecological acceptability, renewability and low risk). Hydrogen is carbon-free fuel which oxidizes to water as a combustion product. The generated water becomes, together with renewable primary energy for splitting it, a source of clean and abundant energy in a carbon-free natural cycle (Momirlan and Veziroglu, 1999).

1.2 Photocatalyst

Photocatalysis is a term that implies the combination of photochemistry with catalysis. Both light and catalyst are necessary to achieve or to accelerate a chemical reaction. In general, what considers a good photocatalyst is that it must possess an optimum energy band for water splitting, strong optical absorption in longer wavelength which is the red shift (visible region), cheap, non-toxic and has good stability in aqueous environment. There are many materials which have small band gaps such as the WO_3, CdS, CdSe, PbS and MoS_2 which are able to absorb light in the visible region. Although these materials meet the criteria of small band gaps, unfortunately the properties of the materials are photoanodic, corrosive and are toxic, therefore are not environmental friendly (Akira and Xintong, 2006). Moreover, metal chalcogenides such as CdS and CdSe, are not stable in water oxidation reaction to form O_2 because the S^{2-} and Se^{2-} anions are more vulnerable to oxidation, causing the CdS or CdSe catalyst to be oxidized and degraded (Kazuhiko and Kazunari, 2007). Therefore, these materials are less favorable to be used as photocatalytic materials. Although WO_3 functions as a stable photocatalyst for O_2 evolution under visible light in the presence of an appropriate electron acceptor, the bottom of the conduction band of the material is located at a more positive potential of water reduction. As a result, the WO_3 does not have the ability to reduce H^+ to H_2. Figure 1.2 depicts a schematic illustration of band structure of some photocatalysts, which presents the above dilemma.

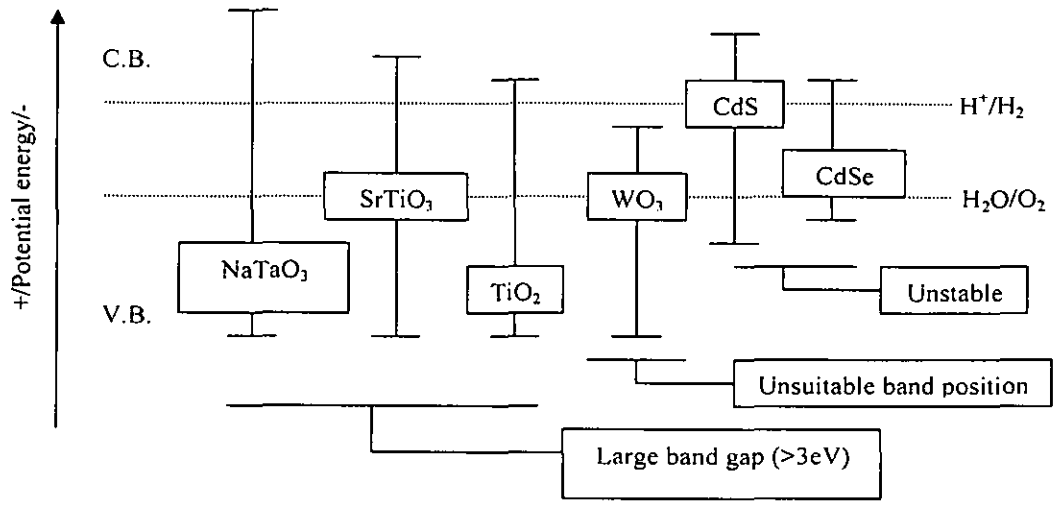

Figure 1.2 Schematic illustrations of band structures of several semiconductor photocatalysts (Kazuhiko and Kazunari, 2007).

Photocatalytic materials like TiO_2, ZnO, $SrTiO_3$ and ZnS have good photostability and are not easily corroded but these materials have relatively wide band gaps and limited light absorption in the visible region and hence low photoactivity. Despite of their large band gaps, many studies have been carried out using these photocatalytic materials. Titanium dioxide is the most popular photocatalyst because of its promising properties and advantages. The pioneering work of Fujishima and Honda in the early 1970s showed that water splitting was possible by illuminating a TiO_2 electrode in an electrochemical cell using sunlight. Since then, much research has been undertaken to develop a suitable photocatalyst material for such applications.

Recently, photohydrogen generation from water utilizing visible light such as solar energy or radiation was studied. The advantage of this reaseach is that hydrogen could be obtained directly from water utilizing solar irradiation (Jae, 2005) which is abundantly available and renewable in nature (Armor, 1999). TiO_2 is one of the photocatalysts that has dominated this field of research and its properties will be discussed in the following sections.

1.3 Titanium Dioxide

Titanium dioxide (TiO_2), also known as titanium(IV) oxide or titania, belongs to the family of transition metal oxides. TiO_2 occurred primarily as minerals such as rutile, anatase, brookite, perovskite and ilmenite. The structure of rutile, anatase and brookite can be discussed in terms of (TiO_2^{6-}) octahedral. The three crystal structures differ by the distortion of each octahedral and by the assembly patterns of the octahedral chains. Anatase can be regarded to be built up from octahedral chains that are connected by their vertices, in rutile, the edges are connected, and in brookite, both vertices and edges are connected (Figure 1.3). Anatase and rutile are the common forms of TiO_2. At normal pressure, rutile is the most thermodynamically stable form of TiO_2 at all temperatures. Anatase, the meta-stable polymorph, changes rapidly to rutile for temperature range 600°C-1000°C depending on the crystallite size and the impurity contents.

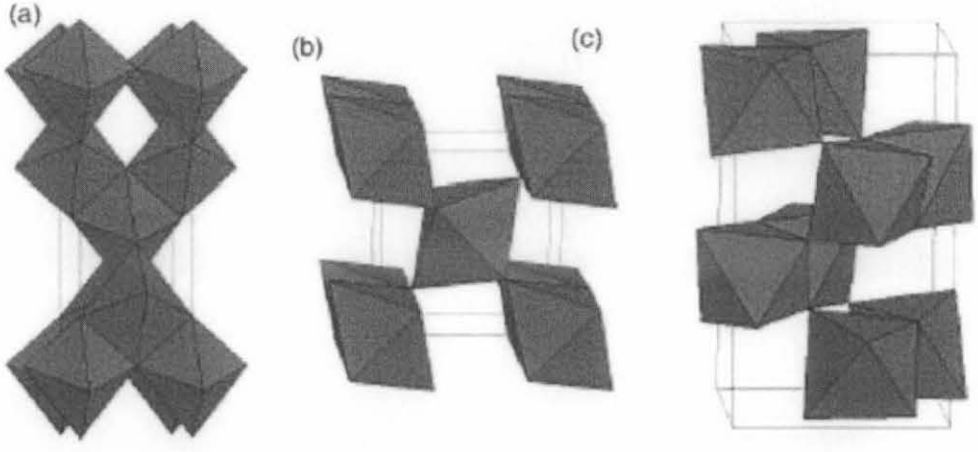

Figure 1.3 Crystal structure of TiO_2 (a) anatase, (b) rutile and (c) brookite (Carp *et al.*, 2004).

Both anatase and rutile are wide band gap semiconductors in which the filled valence band (VB) derived from O 2p orbitals is separated from an empty conduction band (CB) derived from the Ti 3d orbitals. The energy band gaps of anatase is 3.2 eV which corresponds to UV light (388 nm) and rutile is 3.0 eV which corresponds to violet light (413 nm). The anatase phase of TiO_2 has always been used as a photocatalyst due to its

high photocatalytic activity compared to rutile. Its photocatalytic activity is better because the crystal structure, size distribution, porosity, surface hydroxyl group and surface area of anatase are different from rutile (Carp *et al.*, 2004).

TiO_2 has been widely used due to its excellent resistance to chemical and photochemical corrosion in aggressive aqueous environments (Bak *et al.*, 2002; Carp *et al.*, 2004), reactive with both light and water (Carp *et al.*, 2004), which may be attributed to the ease with which the Ti ions (Ti^{3+} and Ti^{4+}) alter their valencies. TiO_2 is substantially less expensive than other photo-sensitive materials, nontoxic and the different processing technologies for TiO_2 production are relatively straightforward and uncomplicated compared to those required for valence semiconductors (Andrea *et al.*, 2007; Maeda and Yamada, 2007; Nowotny *et al.*, 2005). It is used for photocatalytic decomposition of organic compound in water (Masaaki *et al.*, 2007), as white pigment in paints, plastic, papers, leather, pharmaceuticals such as tablet coatings, toothpastes, and as a UV absorber in sunscreen cream with high sun protection factors and other cosmetic products (Carp *et al.*, 2004). The selected applications are also listed in Table 1.2. TiO_2 is also used in catalytic reactions acting as a promoter, a carrier for metals and metals oxides, an additive, or as a catalyst.

Table 1.2 Selected applications of photocatalysis (Carp *et al.*, 2004).

Property	Category	Application
Self-cleaning	Materials for residential and office buildings	Exterior tiles, kitchen and bathroom components, interior furnishings, plastic surfaces, aluminum sidings, building stone and curtains, paper window blinds
	Indoor and outdoor lamps and related systems	Translucent paper for indoor lamp covers, coatings on fluorescent lamps and highway tunnel lamp cover glass.
	Material for roads	Tunnel wall, soundproofed wall, traffic signs and reflectors.
	Others	Tent material, cloth for hospital garments and uniforms and spray coating for cars.
Air cleaning	Indoor air cleaners	Room air cleaner, photocatalyst-equipped air conditioners and interior air cleaner for factories.
	Outdoor air purifiers	Concrete for highways, roadways and footpaths, tunnel walls, soundproofed walls and building walls.
Water purification	Drinking water	River water, ground water, lakes and water and industrial wastewater.
	Others	Fish feeding tanks, drainage water and industrial wasterwater.

Table 1.2 Selected applications of photocatalysis (Carp *et al.*, 2004) (continued).

Property	Category	Application
Self-sterilizing	Hospital	Tiles to cover the floor and walls of operating rooms, silicone rubber for medical catheters and hospital garments and uniforms.
	Others	Public restrooms, bathrooms and rat breeding rooms.
Antitumor activity	Cancer therapy	Endoscope-like instruments

Nevertheless, it is also well known that the powder crystallinity, surface morphology and phase composition determined by given preparation conditions may have a decisive effect on the actual apparent catalytic performance.

For example, among different commercially available titania powders, Degussa P25 shows the highest activity in majority of the photocatalytic H_2 production reactions. Degussa P25 has been in the market for a long time and it has been generally referred to as the standard reference for other titania powders studied. Degussa P25 has high photocatalytic activity due to its unique physical characteristic resulting from its production process. Degussa P25 powder consists of a mixture of anatase and rutile in the proportion of 4:1, is characterized by a specific surface area (SSA) in the order of 50 m^2g^{-1} and particle size of ~20 nm (Kirchernova *et al.*, 2005; Teruhisa *et al.*, 2001). Table 1.3 summarizes the characteristics of Degussa P25 powder.

Table 1.3 Characteristic of Degussa P25 powder (Kirchernova *et al.*, 2005).

Characteristic	Degussa P25
Preparation method	Flame pyrolysis of $TiCl_4$
Composition by XRD	80% anatase, 20% rutile
Apparent powder density (gmL^{-1})	0.05
Primary crystallite size XRD (μm)	30
Morphology	Heterogeneous, wrinkled surface
Apparent particle size (μm)	<10
SSA_{BET} (m^2g^{-1})	50
Weight loss on calcinations (%)	<2 (1237 K)
N_2 adsorption isotherm	Hysterisis from 0.8 to 1 P/P_0
Pore volume (mLg^{-1})	0.15
Pore size distribution	Little porosity, peak at 31.5 nm
Light absorptive characteristics	Peak at about 250 nm
Phase transformation by milling	Fast to rutile only (in 12 h)
Particle size in water (μm)	0.7-10 (70%), 50-100 (10%)
Thermal stability	Increase in rutile content >673 K; lower photocatalytic activity.

Pure TiO_2 is not photoactive under visible illumination because of its wide band gap where the band gap energy, E_g for anatase is 3.2 eV and E_g= 3.0 eV for rutile. This band gap can only absorb near UV-light. Therefore, photocatalytic reactions can only proceed when it receives UV light having wavelength shorter than approximately 388 nm or shorter. However, the use of a photocatalyst that absorbs in visible region is preferable since the solar energy contains large fraction of visible region and only a small fraction of UV region that is 5% for UV, 45% for visible light (wavelength between 400 nm and 800 nm), and 50% for IR (Jae, 2005).

The conduction band (CB) electrons and the valence band (VB) holes recombines very quickly and release energy in the form of unproductive heat or photons and this explained

why the hydrogen production by TiO_2 photocatalytic water splitting is still low (Meng *et al.*, 2007).

In order to overcome the above listed problems, many studies have been done to improve the photocatlytic activity and enhance visible light response of TiO_2 by incorporating an adequate amount of transition metal ions such as Fe, Zn, Cu, Ni and V (Tseng and Wu, 2004). Besides that, addition of some sacrificial electron donors (Gratian *et al.*, 1995) can also enhance the photocatalytic activity of H_2 generation from water (Wu and Lee, 2004).

1.4 Properties of Light

Light is one of the various electromagnetic components present in space. The electromagnetic spectrum covers an extremely broad range, from radio down to X-rays wavelengths. The UV-Visible portion occupies an intermediate position, having both wave and particle properties in varying degrees (Figure 1.4) and Table 1.4 depicts the visible light wavelength and the perceived colours.

1.4.1 UV Light

Short wavelength UV-light exhibits more quantum properties than its visible or IR counterparts. UV light arbitrarily divided into 3 portions, namely UV-A (315-400 nm) which is the least harmful type of UV light, because it has the least energy and is widely used for its relative harmlessness and its ability to cause fluorescent materials to emit visible light, thus appearing to glow in the dark. UV-B (280-315 nm) is the most dangerous form of UV light, because it can damaged biological tissues and causes skin cancer. However, most of the UV-B light is filtered by the ozone layer before penetrating to the atmosphere. As for UV-C (100-280 nm) it is almost completely absorbed in air within few hundred meters. When UV-C photons collided with oxygen atoms, the energy exchange causes the formation of ozone (O_3).

1.4.2 Visible Light

Visible light is concerned with the radiation perceived by human eyes. Typical human eyes will respond to wavelengths in air from about 380 to 750 nm. Yellowish-green light receives the greatest weight because it simulates the eye more than the blue or red light of equal radiometric power (1 W at 553 nm = 683 lumens).

1.4.3 Infrared Light

IR light contains the least amount of energy per photon of any other band and is unique in that it has primarily wave properties. This can make it much more difficult to manipulate than UV and visible light. IR light is more difficult to focus with lenses, refract with lenses, diffract more and is difficult to diffuse. Since IR light is a form of heat, far IR detectors are sensitive to environmental changes such as a person moving in the field of view. Night vision equipment takes advantage of this effect, amplifying IR to distinguish people and object that are concealed in dark.

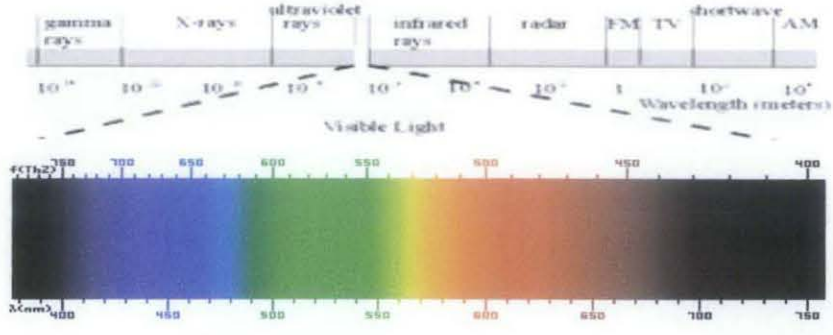

Figure 1.4 Light spectrums.

Table 1.4. Visible light wavelength and perceived colour.

Wavelength Range (nanometers)	**Perceived Color**
340-400	Near Ultraviolet (UV; Invisible)
400-430	Violet
430-500	Blue
500-570	Green
570-620	Yellow to Orange
620-670	Bright Red
670-750	Dark Red
Over 750	Near Infrared (IR; Invisible)

1.5 Objectives

The aim of this study is:-

a) To develop Cu/TiO_2 photocatalysts for hydrogen production from water under visible light.

CHAPTER 2

LITERATURE REVIEW

2.1 Modification of Photocatalyst to Reduce TiO_2 Band Gap

In order to enhance the absorption of TiO_2 photocatalyst towards the visible region, modification of the properties of the catalyst surface can be achieved by metal doping, non-metal doping and also dye sensitization to enhance TiO_2 adsorption region. Other approaches like ion implantation and semiconductor coupling have also been investigated by other researchers. All these techniques of modification could reduce the band gap of TiO_2 and induce visible light response. Through metal doping technique, several photocatalytic applications could be performed under longer wavelengths in the visible light spectrum as shown in previous chapter (Table 1.4). Non-metal doping technique on the other hand has incorporated elements such as N, C, S, P, B and oxygen into TiO_2 lattice (Akira and Xintong, 2006; Meng *et al.*, 2007). Of the various non-metals, nitrogen is most frequently used to improve visible light absorption. Preparation methods such as spray pyrolysis (Li *et al.*, 2005), sputtering (Premkumar, 2004), pulsed laser deposition (Suda *et al.*, 2004), sol-gel (Livraghi *et al.*, 2005) and mechanochemistry technique (Livraghi *et al.*, 2005) were commonly used to prepare N-doped TiO_2. Transition metal doping technique has employed metals such as Cu (Andrzej, 1991; Colon *et al.*, 2006; Ha *et al.*, 2006; Komova *et al.*, 2000; Maeda and Yamada, 2007; Slamet *et al.*, 2005; Tseng *et al.*, 2002; Tseng and Wu, 2004; Xin *et al.*, 2008), Ni (Ann *et al.*, 1998; Dong *et al.*, 2005; Dong *et al.*, 2008; Goncalves *et al.*, 2006; Jolanta *et al.*, 2003; Sayama *et al.*, 1996; Sun *et al.*, 2006; Wu *et al.*, 2005), Cr (Dana *et al.*, 2002; Dong *et al.*, 2004; Paola *et al.*, 2001), Fe (Dong *et al.*, 2004), Ag (Park and Kang, 2008) and Zn (Meng *et al.*, 2007).

2.1.1 Transition Metal Incorporation

Doping has often been attempted to prepare visible light driven photocatalysts. Here, doping often means replacement of a crystal lattice point in TiO_2 photocatalyst with a foreign element (Akihiko *et al.*, 2007). Doping with a foreign element such as transition metal ions into a photocatalyst is one of the strategies that can affect the morphology such as the particle size and surface structure of photocatalyst particles (Akihiko *et al.*, 2007; Jing and Guo, 2007). A dopant ion might act as an electron trap and lead to a longer lifetime of the generated charge carriers thus results in enhancement of the photocatalytic system (Akihiko, 2003). The incorporation of the dopant may be deposited on the surface of the support, incorporated into the interior of the particle or may form separate oxides. These factors can be controlled by changes in pretreatment conditions, dopant loadings or preparation methods such as wet impregnation (Hyung and Misook, 2007), deposition-precipitation and sol-gel (Colon *et al.*, 2006; Wu and Chih, 2001; Lei *et al.*, 2006; Maeda and Yamada, 2007; Min *et al.*, 2007).

On the other hand, doping of transition metal cations into photocatalysts with wide band gaps such as TiO_2 and $SrTiO_3$ has been studied for a long time in the research field of photoelectrochemistry and photocatalysis in order to modify electronic structure and develop materials with visible light response. This method of improving photocatalytic activity is mainly used in aqueous media (Carp *et al.*, 2004). For instance, TiO_2 particles can be substitutionally doped with different cations that can form mixed oxide or mixture of oxides. The dominant parameters involved the character and concentration of dopants and the applied thermal treatment. The effect of this alteration could change the light absorption capability of the TiO_2 photocatalyst, the adsorption capacity of the substrate molecules at the catalyst surface and interfacial charge transfer rate (Carp *et al.*, 2004; Wilke and Breuer, 1999; Xu *et al.*, 2004).

The requirements for splitting water into H_2 and O_2 by semiconductor photocatalysts are related to the band structure, in which the bottom of a conduction band level is more negative than the redox potential of H^+/H_2 (0 V vs. NHE method) and the top valence

band is more positive than the redox potential of O_2/H_2O (1.23 V vs. NHE). Valence band levels of metal oxide photocatalysts with d^0 or d^{10} configuration are too positive (ca. 3 V vs. NHE) compared with the redox potential of O_2/H_2O. Therefore, the band gaps of photocatalysts for water splitting are inevitably wider than 3 eV. These photocatalysts respond only to UV radiation. Therefore, the objective for doping is to induce a batho-chromic shift (decrease of band gap or introduction of intra-band gap states, which results in more visible light absorption) (Carp *et al.*, 2004). Transforming new valence bands or electron donor levels above the valence band consisting of O 2p orbitals is indispensable to develop visible light responsive photocatalysts. If a dopant forms an electron donor level in the band gap of a host semiconductor photocatalyst, the photocatalyst may show visible light response as shown in Figure 2.1 (Akihiko *et al.*, 2007). This idea is applied to photocatalyst with UV response such as TiO_2, ZnS, $NaTaO_3$ and WO_3.

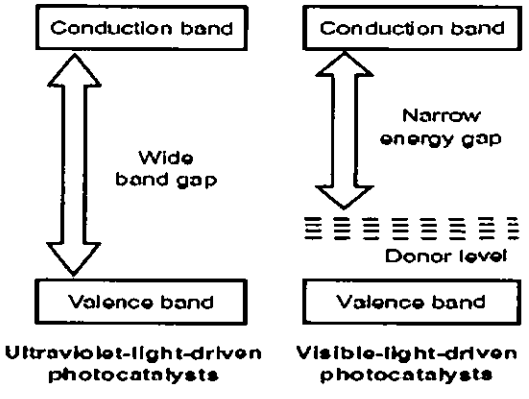

Figure 2.1 Visible-active photocatalysts obtained by doping to reduce band gap (Akihiko *et al.*, 2007).

Noble metals such as Pt, Au, Pd and Rh and transition metals such as Ni, Cu and Ag, have been reported to be very effective for enhancement of TiO_2 photocatalyst (Gratian *et al.*, 1995; Sakthivel *et al.*, 2004; Wu *et al.*, 2004; Zhou *et al.*, 2006) towards visible light absorption. Doping of these metals could also greatly reduce the possibility of electron-hole recombination, resulting in efficient separation and stronger photocatalytic reactions.

The most frequently used metal for hydrogen generation was Pt (Anpo and Takeuchi, 2003; Gratian *et al.*, 1995) which is very efficient but expensive. Therefore, cheaper and easily available alternatives were sought to substitute Pt, such as transition metals (e.g. Cu, Ni, Ag and Cr). According to Dhanalakshimi *et al.* (2001), an investigation for hydrogen production was carried out between dye-sensitized, Pt/TiO_2 and Cu/TiO_2 photocatalysts. The result for hydrogen production from Cu/TiO_2 loading was almost comparable from Pt/TiO_2 loading. Therefore, intensive study by incorporating these inexpensive but effective transition metals for the enhancement of photocatalytic activity should be carried out.

Investigation on indium-tantalum-oxide doped with $Ni/In_{0.9}NiO_{0.1}TaO_4$ supported with NiO_x or RuO_2 as the promoter was developed by Zou *et al.* (2002). In their study, the prepared photocatalysts were able to induce the direct water splitting into H_2 and O_2 under visible light irradiation ($\lambda > 420$ nm), where the partially filled Ni 3d shell plays an important role in modifying the electronic properties of $InTaO_4$. The absorption band in the range of 420-520 nm was observed for the Ni-doped compound. Photocatalytic H_2 production using NiO loaded onto mixed oxide photoacatalysts have been conducted (Heondo *et al.*, 2006; Hideki and Akihiko, 1999; Ko and Lee, 2002; Lin *et al.*, 2007; Zou *et al.*, 2002). For instance, Ko and Lee (2002) have developed 2.7 wt% $NiO\text{-}Sr_4Ti_3O_{10}$ photocatalyst for H_2 production. In their study, the photocatalyst was suspended into distilled water and irradiated with 400 W of high pressure Hg lamp and the H_2 evolved was 170 $\mu molh^{-1}$. A similar reaction study was also carried out by Heondo *et al.* (2006) using 3 wt% $NiO\text{-}Sr_4Ti_2O_7$ prepared by polymerized complex method (PCM) and 3 wt% $NiO\text{-}Sr_4Ti_2O_7$ prepared by solid state reaction method (SSRM). From their results, the H_2 evolution was 144 $\mu molh^{-1}$ for 3 wt% $NiO\text{-}Sr_4Ti_2O_7$ (PCM) and 77 $\mu molh^{-1}$ for 3 wt% $NiO\text{-}Sr_4Ti_2O_7$ (SSRM). Zou *et al.* (2002) reported that the NiO_x loaded onto $In_{0.9}Ni_{0.1}TaO_4$ photocatalyst for H_2 production with pure water under the irradiation of 300 W Xe arc lamp was 16.6 $\mu molh^{-1}$. Photocatalytic H_2 production using 1 wt% $NiO/InVO_4$ photocatalyst was investigated by Lin *et al.* (2007). According to these authors, the reaction was carried out using 0.1 g of photocatalyst suspended in 50 mL of distilled water and irradiated with 500 W halogen lamp. The H_2 evolved was 896 $\mu molh^{-1}$.

Visible light active photocatalysts $NaTaO_3$ have also been studied for water splitting into H_2 and O_2. Doping of La, Ca, Sr and Ba into $NaTaO_3$ was successfully developed by Akihiko *et al.* (2007). According to their investigation, the dopants changed the morphology of $NaTaO_3$ particle. The decrease in the particle size and the formation of characteristic surface nanostep structure resulted in excellent photocatalytic performance. On the other hand, doping of Cr, Ni, Cu, Rh and Pb proved effective for development of visible light responsive photocatalysts based on TiO_2, $SrTiO_3$ and ZnS with wide band gaps (Akihiko *et al.*, 2007). These doped photocatalyst showed activities for H_2 and O_2 evolution from aqueous solutions containing sacrificial reagent. The absorption band for these doped photocatalyst was observed in the range of 420-550 nm. In addition, Mg-doped WO_3 photocatalyst could also induce water splitting in the presence of methanol as sacrificial agent under visible light irradiation ($\lambda > 400$ nm) (Dong *et al.*, 2002). Further study by other researchers investigating photocatalyst based on $La_2Ti_2O_7$ synthesized via conventional solid-state reaction was also developed by Dong *et al.* (2004) for similar studies using Cr and Fe as the dopants. The results showed intense absorption in the visible region ($\lambda > 400$ nm) for these photocatalysts.

The doping of TiO_2 photocatalysts with metal ions such as Cr, Fe, V and Ni via metal ion implantation was demonstrated by Masakazu (1997). In this study, the implantation of these metal ions to modify the electronic properties of the semiconductors by bombarding these metals ions with high voltage. The absorption band of the TiO_2 photocatalysts implanted with metal ions such as Cr, V, Fe and Ni were found to shift to visible regions. This technique was found to be capable of absorbing visible light up to 550 nm. Similar study was investigated by Masaaki *et al.* (2007) which reported that, incorporation of V, Cr, Fe and Ni onto TiO_2 by ion implantation and impregnation method showed significant shift to the visible light region (up to 600 nm) as compared to the undoped TiO_2 (Figure 2.2).

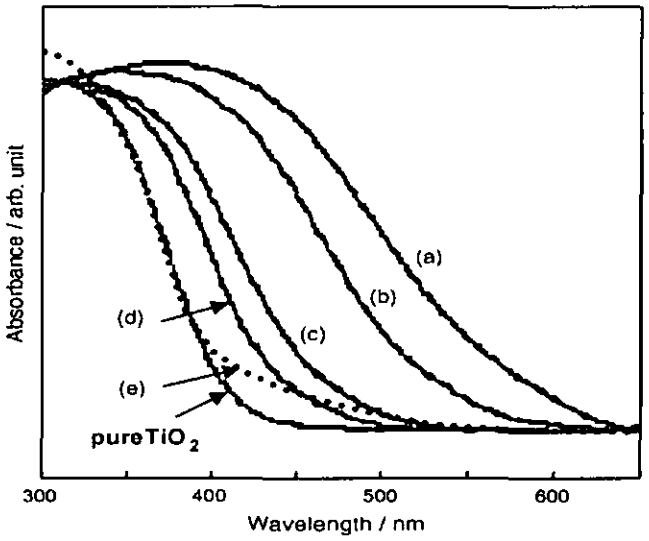

Figure 2.2 Diffuse reflectance UV-Vis spectra of the TiO_2 photocatalyst implanted with (a) V, (b) Cr, (c) Fe, (d) Ni and (e) Cr prepared by impregnation method (Masaaki *et al.*, 2007).

In another study, the incorporation of (0.5-5 wt %) Ni ion onto TiO_2 via sol gel could also enhance photocatalytic H_2 production under the visible light irradiation as reported by Thammanoon *et al.* (2005). It is observed that the diffuse reflectance spectra of the absorption band were shifted to a longer wavelength between 600 nm and 800 nm upon the incorporation of NiO/TiO_2. TiO_2 on the other hand has the band edge near 350 nm. Based on Thammanoon's study, the NiO served as electron (e^-) trapper and prohibits the recombination of holes and electrons.

Development of visible responsive photocatalyst for H_2 production was investigated using Cu. For example, the investigation on CuO/TiO_2 photocatalysts by Bandara *et al.* (2005) for H_2 production via wet impregnation method was found to be capable to shift the absorption edge of TiO_2 into longer wavelength (420-600 nm) compared to bare TiO_2 which absorbs only in UV region. Photocatalytic H_2 production was reported to perform better under visible light using CuO/TiO_2 compared to TiO_2 only. Similar study was also carried out by Hyung and Misook (2007) using CuO/TiO_2 with the addition of sacrificial

reagent in which H_2 production was markedly enhanced. Results from both studies were coherent in which incorporation of Cu could enhance the photocatalytic reaction.

Dye-sensitized CuO/TiO_2 could enhance photocatalytic hydrogen production compared to non dye-sensitized photocatalyst under the radiation of visible light (Jin *et al.*, 2007) According to these authors, Eosin Y sensitized CuO/TiO_2 photocatalyst was active and stable for H_2 generation under the visible light region, as evidenced by the absorption band from 450-650 nm of the diffused reflectance spectra. Further study using reduced CuO was developed by Yasomanee and Bandara (2008) supported on TiO_2 prepared via thin film. Photocatalytic reaction was carried out using a solar simulator. Interestingly, the H_2 production was observed even in dark condition but at a lower production rate for up to 2 hours. According to these authors, the irradiation of Cu_2O/TiO_2 led to the formation of trapped electrons and this stored energy is used to generate H_2 from H_2O in the dark. However the H_2 production was not observed for TiO_2.

2.2 Addition of Sacrificial Reagent to Enhance Photocatalytic Activity

The photocatalytic reaction for H_2 production can also be influenced by the presence of some organic and inorganic species in the reacting system. Such species are known as the "sacrificial reagent" or "scavengers". The addition of sacrificial reagent has been investigated and found to be able to suppress the instantaneous recombination of the electron and hole pairs. Among the sacrificial reagents that have been reported in the literature are methanol, ethanol, EDTA, Na_2CO_3 (Sayama and Arakawa, 1996), NaOH (Hironori and Kazuhiko, 2000; Sayama *et al.*, 1990) and lactic acid (Meng *et al.*, 2007). Addition of these sacrificial reagents proved to be effective to enhance the photocatalytic reaction and prolong the lifetime of the electron-hole separation (Gratian *et al.*, 1995; Gurunathan *et al.*, 1997; Kida *et al.*, 2004; Lee *et al.*, 2001; Li *et al.*, 2003; Nada *et al.*, 2005; Wu *et al.*, 2004). The addition of NaOH for H_2 and O_2 generation from water was conducted by Sayama *et al.* (1990) using 0.1 wt% NiO-loaded $K_4Nb_6O_{17}$ photocatalyst irradiated under 450 W of high pressure Hg lamp. Similar study employing NaOH, NaCl and Na_2SO_4 in the aqueous suspension of Pt/TiO_2 for H_2 and O_2 production was also

investigated by Hironori and Kazuhiko (2000) but only slight increase of H_2 production was observed in the photocatalytic reaction. Moreover, when Na_2CO_3 was used as the sacrificial agent, H_2 evolution improved drastically compared to NaOH, NaCl and Na_2SO_4. Similar photocatalytic H_2 production was also studied by Sayama and Arakawa (1996) using ZrO_2 photocatalyst under the illumination of 400 W high pressure Hg lamp.

2.2.1 Addition of Electron Donors

Due to rapid recombination of photogenerated CB electrons and VB holes, addition of electron donors can reduce the photocatalytic electron/hole recombination resulting in higher photocatalytic activity (Meng *et al.*, 2007).

Hydrogen production using Ag supported onto TiO_2 with the addition of methanol as sacrificial reagent was investigated by Park and Kang (2008) under the UV irradiation. According to them, the H_2 production over Ag/TiO_2 prepared by sol-gel was 713.5 $\mu molh^{-1}$ compared to TiO_2 which yield only 136.66 $\mu molh^{-1}$. Photocatalytic H_2 production using supported noble metal such as Ru (Nada *et al.*, 2005) and Pt (Anna and Jerzy, 2005; Yi *et al.*, 2008) was investigated for water-methanol system. Pt/TiO_2 photocatalyst prepared via wet impregnation was carried out for the H_2 production by Anna and Jerzy (2005). The photoacatalyst was irradiated with 450 W medium pressure Hg lamp and the H_2 production was 6.59 mmol. Similar study was investigated by Yi *et al.* (2008) which reported that the addition of this sacrificial reagent into the aqueous suspension of Pt/TiO_2 prepared through photodeposition technique, significantly improved the H_2 production under the illumination of 500 W high pressure Hg lamp. Photocatalytic H_2 production under this system was 9112 $\mu molh^{-1}$. However the photocatalytic performance in this study was incomparable due to the different parameters used. As for Ru supported onto TiO_2 prepared via wet impregnation, the photocatalytic H_2 production was 18.166 $\mu molh^{-1}$ (Nada *et al.*, 2005). Besides methanol, ethanol was also used as sacrificial electron donor for hydrogen production. Noble metal such as Au and Pt supported onto TiO_2 photocatalyst was prepared by deposition-precipitation, impregnation and photodeposition. As reported by Gratian *et al.* (1995), H_2

production performed better using Pt/TiO_2 compared to Au/TiO_2 prepared by deposition-precipitation where the H_2 produced were 25.714 x 10^3 $molh^{-1}$ and 32.857 x 10^3 $molh^{-1}$, respectively.

So far, several approaches for development of photocatalysts utilized for H_2 in water-MeOH system have been examined not only with TiO_2 but also with other mixed oxides supports such as $K_4Nb_6O_{17}$, $NaTaO_3$, Nb_2O_3, Ta_2O_6 and $InVO_4$. For example, Ye *et al.* (2003) studied the difference between Ni/Nb_2O_3 and Ni/Ta_2O_6 photocatalysts for H_2 production using 400 W of high pressure Hg lamp. According to their report, the amount of H_2 collected were 260 $\mu molh^{-1}$ for Ni/Ta_2O_6 and 180 $\mu molh^{-1}$ for Ni/Nb_2O_3. Different power for the light source (300 W Xe lamp) was also studied by Ye and coworkers without the addition of MeOH as the scavenger. The results were not promising as the amount collected were 0.168 $\mu molh^{-1}$ for Ni/Nb_2O_3 and 0.208 $\mu molh^{-1}$ for Ni/Ta_2O_6. Masaya *et al.* (2007) investigated on 0.1 wt% $NiO/K_4Nb_6O_{17}$ photocatalyst employed in H_2 production using the water-MeOH system under the irradiation of 450 W high pressure Hg lamp. The amount of H_2 produced was 667 $\mu molh^{-1}$.

Photocatalytic H_2 production from water (with addition of 5 v/v% methanol) was studied by Bandara *et al.* (2005) using CuO supported TiO_2 under the irradiation of 125 W medium pressure Hg lamp. The H_2 production from photocatalyst prepared by wet impregnation was 20 mLh^{-1} for 10 wt% CuO/TiO_2 and 0.63 mLh^{-1} for bare TiO_2. The photocatalytic reaction was found to be active and stable for H_2 production under the water-MeOH system. Photocatalytic H_2 production using this sacrificial reagent was also studied by Hyung and Misook (2007). In their investigation, copper photocatalyst supported on TiO_2 with loading of 1, 5 and 10 wt% were prepared by conventional impregnation. Photocatalytic reaction was studied by using volume ratio of 1:1 water-MeOH mixture. A marked increased of H_2 production was observed for 10 wt% Cu/TiO_2 (1350 $\mu molh^{-1}$) followed by 5 wt% Cu/TiO_2 (700 $\mu molh^{-1}$) and 1 wt% Cu/TiO_2 (100 $\mu molh^{-1}$). Similar study was performed by Jeon *et al.* (2007) on the photocatalytic activity of Cu/TiO_2 prepared by sol-gel method. The highest H_2 evolution was achieved at 688.33 $\mu molh^{-1}$ for rutile Cu/TiO_2 and 644.71 $\mu molh^{-1}$ for anatase.

2.3 Mechanism of Photocatalytic Water-splitting or Hydrogen Production

The electronic structure of a semiconductor plays an important role in semiconductor photocatalysis. A semiconductor consists of valence band (VB) and conduction band (CB). Energy difference between these two levels is said to be the band gap (E_g) (Meng *et al.*, 2007; Senevirathna *et al.*, 2005). The photocatalytic water-splitting can be explained using the TiO_2 photocatalyst mechanism (Bandara *et al.*, 2005; Jin *et al.*, 2007). Without excitation, both the electrons and holes are in the valence band. During the excitation, absorption of photons with energy greater than the band gap energy of TiO_2 instigates the formation of conduction band electrons (e^-) and valence band hole (h^+), which migrate towards the TiO_2 surface (Figure 2.3). For photocatalyst TiO_2, the reaction is expressed as:

$$TiO_2 \xrightarrow{hv} e^-_{TiO_2} + h^+_{TiO_2} \qquad (2.1)$$

The excited electrons (Equation 2.1) can rapidly transport to the loaded catalyst actives sites and reduce $H^+ \rightarrow H_2$ (reducible adsorbates) in the solution to generate hydrogen, which subsequently diffuses through the aqueous phase and emerges into the gaseous phase. Concomitantly, the holes can be removed by reacting with the hole scavenger (e.g. methanol), in order to prevent unfavorable electron-hole recombination process (Thammanoon *et al.*, 2005).

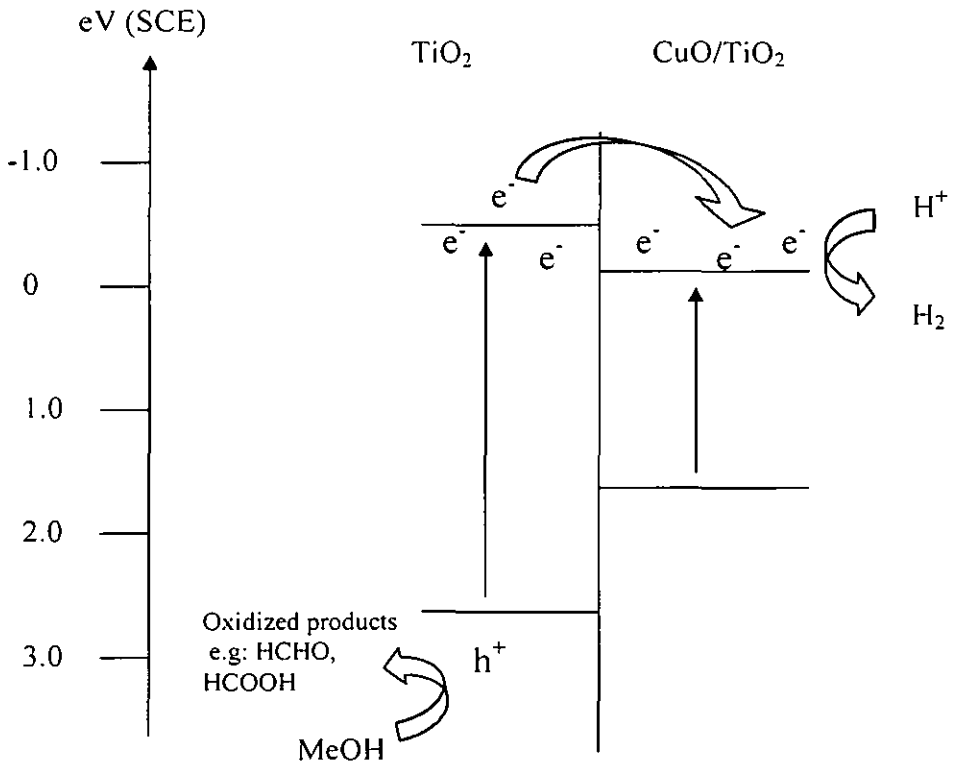

Figure 2.3 Schematic diagram for the photocatalytic H_2 production (Bandara *et al.*, 2005; Jin *et al.*, 2007).

2.4 Band Gap Determination from Diffuse Reflectance Measurement

Diffuse reflection occurs when the incident radiation penetrates into the sample powder and gets reflected by grain boundaries of the particles. Diffuse reflectance depends on the particle size and when the particle size decreases, the number of reflections at the grain boundaries increases. As a result, the depth of penetration of the incident light decreases in the absorbed portion of light and increases in the reflected portion of light. On increasing the particle size, the depth of penetration increases, as a result of less grain boundary reflections and hence the reflectance decreases (Jeevanandam *et al.*, 2007).

Kubelka-Munk (KM) theory is widely accepted for explaining the optical properties of complex powder system and the theory is shown in equation 2.2.

$$F(R_\infty) \equiv \frac{(1-R_\infty)^2}{2R_\infty} = \frac{K}{S} \qquad (2.2)$$

where,

K is the absorption coefficient,

S is the scattering coefficient and

R_∞ is the reflectance of the sample at the infinite thickness.

F(R) is called the KM function, also called the remission function (Carl and Allen, 1997; Jeevanandam *et al.*, 2007; Joachim *et al.*, 1997; Lacey and Peter, 2006; Zaghib *et al.*, 2007). The optical band gap is determined from the KM formalism for diffuse reflectance R by extrapolating F(R) to the zero-energy axis. For a semiconductor, the Tauc's plot $[F(R).h\nu]^n$ versus photon energy will show a linear region just above the optical absorption edge for n=1/2 if the band gap is direct transition, or n=2 if the band gap is indirect. The relationship of this plot can be described by the following formula:

$$[F(R).h\nu]^{1/2} = A(h\nu - E_g) \qquad (2.3)$$

where,

$h\nu$ is photon energy and

E_g is the apparent optical band-gap energy and

A is the characteristic constant of semiconductors

From equation 2.3, $[F(R).h\nu]^{1/2}$ has a linear relationship with $h\nu$. Extrapolation of this line to photon energy ($h\nu$) axis yields the semiconductor band gap when $[F(R).h\nu]^{1/2} = 0$ (Murphy, 2007; Yuan *et al.*, 2006; Zaghib *et al.*, 2007).

CHAPTER 3

METHODOLOGY

In this study, Cu/TiO_2 photocatalysts were prepared employing two methods which is the complex-precipitation and wet impregnation method. Degussa P25 (Aerosil Germany) TiO_2 photocatalyst (predominantly anatase with specific surface area of 50 m^2g^{-1}) was used as a support in this study. Copper nitrate trihydrate purchased from Acros with 99% purity was used as the copper precursor for the photocatalyst preparation. Sodium hydroxide was used as the precipitating agent. For the complex-precipitation method glycerol was added during the complex-precipitation method. For all photocatalytic reaction, methanol was used as the sacrificial reagent. All the chemicals are listed in Table 3.1 and were used without further purification. The photocatalysts were characterized using the equipments listed in Table 3.2.

Table 3.1 List of chemicals used.

Chemicals	Brand name	Purity
Copper nitrate trihydrate [$Cu(NO_3)_2.3H_2O$]	Acros	>98%
Titanium dioxide (TiO_2)	Degussa P25	80% anatase; 20% rutile
Glycerol	Systerm	95%
Sodium hydroxide (NaOH)	Merck	95%
Methanol	Systerm	95%

Table 3.2 List of equipments used.

Equipments	Model
Temperature Programmed Desorption, Reduction and Oxidation (TPDRO)	Thermo Finnigan 1100
Diffuse Reflectance UV-Vis spectrophotometer (DR-UV-Vis)	Shimadzu 3150
Field Emission Scanning Electron Microscope (FE-SEM)	LEO
Thermo Gravimetric Analysis (TGA)	Perkin Elmer
Fourier Transform Infared (FTIR)	Shimadzu
X-ray Diffractometer (XRD)	BRUKER D8 AXS
Surface Area Analyzer	Autosorb-1C
Drying oven	CARBOLITE
Muffle furnace	STRUART
Multi reaction port	Custom made

3.1 Photocatalyst Preparation and Pretreatment

A series of Cu/TiO_2 photocatalysts were prepared with 2, 5, 10 and 15 wt% Cu loading using complex-precipitation and wet impregnation methods. Both methods were carried out at room temperature.

3.1.1 Preparation of Cu/TiO_2 Photocatalyst by Complex-precipitation method

Appropriate amounts of $Cu(NO_3)_2.3H_2O$ and TiO_2 were weighed into separate beaker. The copper salt was dissolved in 200 mL of distilled water and glycerol was added to this beaker (Cu: glycerol of 1:2 mol ratio) and continuously stirred with a magnetic stirrer. While stirring, the TiO_2 support was added into the solution to form a suspension. Further dropwise addition of 140 mL of 0.25 M NaOH into the suspension was carried out with continuous stirring. The precipitate formed was left to stir for another 30 min before it was filtered and dried at 70°C in an oven overnight (18 hours). Calculation for the preparation of 0.25 M NaOH preparation is provided in Appendix A. Prior to calcination,

thermal decomposition analysis of the 10 wt% Cu/TiO_2 dried catalyst was conducted using a thermal gravimetric analyzer. Results derived from the thermogram were used to determine suitable calcination temperatures. Calcination of the dried supported precursor were done in a muffle furnace at 300, 400 and 500°C for 30 min deduced from the thermogram and designated as mCuGT*x* where *x* is calcination temperature (x 100°C) and m is the Cu loading for the precursor (in wt%). For instance, the copper-complex precipitation with 10 wt% copper supported onto TiO_2 calcined at 300°C for 30 min was designated as 10CuGT3_30. Table 3.3 summarizes the amount of materials used to prepare the photocatalysts. Detailed calculation is provided in Appendix B.

Table 3.3 Summary of the materials used for complex-precipitation.

	Cu loading, wt%			
	2	5	10	15
Mass of $Cu(NO_3)_2.3H_2O$, g	0.7615	1.9039	3.8077	5.7112
Total mass of TiO_2, g	9.8	9.5	9	8.5
Total volume of glycerol, mL	0.5	1.2	2.3	3.5
Total volume of distilled water, mL	40	100	200	300
Total volume of (10 wt/v %) NaOH, mL	28	70	140	210

3.1.2 Preparation of Cu/TiO_2 Photocatalyst by Wet Impregnation method

An adequate amount of $Cu(NO_3)_2.3H_2O$ and TiO_2 were weighed in a beaker according to the metal loading required. The copper nitrate salt was dissolved into 100 mL of distilled water with continuous stirring. Then, the TiO_2 support was added into the copper nitrate solution. The suspension was stirred for 1 hour before the solvent was evaporated in a water bath at 80°C and further dried in an oven at 120°C for 18 hours. Prior to calcination, a thermal decomposition analysis of the 10 wt% Cu/TiO_2 dried supported precursor was carried out to determine the suitable temperatures for calcination. Calcination of the dried supported precursor were done in a muffle furnace at 300, 400 and 500°C for 30 min and designated as mCuT*x* where *x* is calcination temperature (x 100°C) and m is the Cu

loading for the precursor. Table 3.4 summarizes the amount of materials used to prepare the photocatalysts.

Table 3.4 Summary of the amount of materials used for wet impregnation.

Conditions	Cu loading, wt%			
	2	5	10	15
Mass of $Cu(NO_3)_2.3H_2O$, g	0.76151	1.9039	3.8077	5.7112
Total mass of TiO_2, g	9.8	9.5	9	8.5
Total volume of distilled water, mL	100			

3.2 Characterization of Photocatalyst

Characterization of the calcined samples was carried out to determine the physical and chemical properties of the photocatalysts. This was conducted using thermal gravimetric analysis, powder X-ray diffraction analysis, Fourier transform infrared spectroscopy, BET surface area determination, diffuse reflectance spectroscopy, field emission scanning electron microscopy and temperature programmed reduction (Figure 3.1).

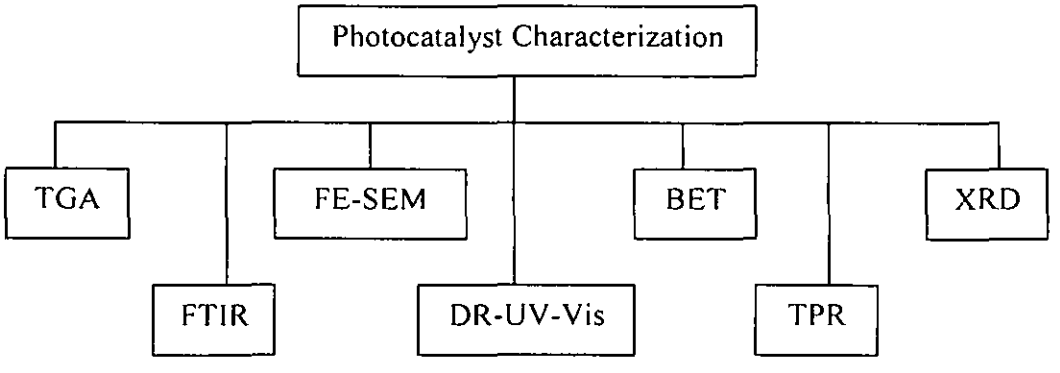

Figure 3.1 An overview of the characterization of the photocatalyst.

3.2.1 Thermal Gravimetric Analysis

For pretreatment of the photocatalysts, thermal gravimetric analyses (TG) were carried out using Perkin Elmer TG (Pyris 1) system to determine the approximate decomposition temperature of Cu-glycerol complex and Cu nitrate salts present in the dried supported precursor. These dried supported precursors were weighed in the range of 5-10 mg using a built-in microbalance attached in the instrument which automatically read the weight of the sample. The samples were heated from 30°C to 800°C at a ramp rate of 20°Cmin^{-1} under flowing air at 20 mLmin^{-1}.

3.2.2 Fourier Transform Infrared (FTIR)

The FTIR spectra of the Cu/TiO_2 catalysts with various calcination temperatures were scanned from 4000 cm^{-1} to 450 cm^{-1} by Perkin Elmer Spectrophotometer. Approximately 1 mg of each powder sample was grained with 200 mg of IR-grade KBr. The samples were then transferred into a die and were pressed into a pellet using a hydraulic hand press. Later the pellet was placed in a sample holder and scanned using the FTIR instrument.

3.2.3 Diffuse Reflectance UV-Vis (DRS)

Diffuse Reflectance UV-Vis spectra of the Cu/TiO_2 photocatalysts were recorded on a Perkin Elmer Lambda 900 with an integrating sphere attachment, using Ba_2SO_4 powder as an internal reference. The powder for each sample was filled into a sampling void of a sample holder and its surface smoothened. The layer have to be infinitely thick that all incident light is absorbed or scattered before reaching the back surface of the sample; typically a thickness of 1-3 mm is required. Reflectance spectra were collected as $R= R_{sample}/R_{reference}$, then plotted as the remission function, $F(R) = (1-R)^2/2R$ (based on the Kubelka-Munk theory or diffuse reflectance). As mentioned in Section 2.4, the band gaps for all the photocatalysts were determined from the extrapolation of the absorption edge onto the energy axis (E_g).

3.2.4 Surface Area Determination

The surface analyzer (Quantachrome Autosorb-1C) using Brunauer-Emmet-Teller (BET) method is widely used for the physical adsorption of gas molecules on a solid surface. The surface area, pore volume, average pore size and pore size distribution of the photocatalyst can be determined from adsorption isotherms. This method is based on multipoint nitrogen adsorption-desorption principle. A sample contained in an evacuated sample tube is cooled to cryogenic temperature (-196°C) and exposed to analysis gas at a series of precisely controlled pressures. The number of gas molecules adsorbed on the surface increases with each incremental pressure. The pressure at which adsorption equilibrium occurs is measured and the universal gas law is applied to determine the quantity of gas adsorbed.

The BET surface area of the photocatalysts was determined using a surface analyzer (Quantachrome Autosorb 1C) located in AMREC, Kulim. For each analysis approximately of 0.1-0.3 g of sample was weighed into a sample tube. Prior to the analysis, each photocatalyst sample was degassed at 130°C overnight (18 hours) to ensure that there was no adsorbed moisture on the photocatalyst surface. The dewar cold trap was filled with liquid nitrogen to trap impurities in the manifold. After degassing, the sample was left to cool to room temperature under vacuum condition. Before the sample tube can be safely removed from the degassing port, the tube need to be backfilled with nitrogen gas. The sample tube was reweighed to determine the actual sample mass which was keyed into the software. Subsequently, it was placed into the analysis port and secured by a connector nut, ferrule and o-ring. The sample cell was immersed in liquid nitrogen in a dewar flask on an elevator. The sample information was then fed into the software to start the analysis.

3.2.5 Field Emission Scanning Electron Microscopy (FE-SEM)

The morphologies of the samples were determined by FE-SEM (LEO 1543) located at AMREC, Kulim. An adequate amount of samples were placed on the studs. The samples

were then coated with a layer of platinum. Later the coated samples were placed into the instrument for scanning. The morphologies of the prepared samples were observed using scanning electron microscopy with the following settings:-

EHT	: 10 kV
Working distance	: 2-4 mm
Magnification	: 100 KX

3.2.6 Temperature Programmed Reduction (TPR)

Catalysts were characterized by Temperature Programmed Reduction (TPR) method. The TPR measurements were carried out using Thermo Finnigan TPDRO 1100 equipment. TPR analysis used to determine the quantity of reducible species present in the catalyst and the temperature at which the reduction itself takes place (Shi *et al.*, 2004). Samples were loaded in a quartz U-tube reactor. Approximately 0.1-0.2 g of sample was used for each measurement. Prior to reduction, the sample was pretreated under nitrogen at 110°C with a flow rate of 20 $mLmin^{-1}$ and ramp rate of 10°$Cmin^{-1}$, and finally holding at 110°C for 10 min to eliminate moisture before cooling to room temperature. TPR was carried out in 5% H_2 in N_2 from 40°C-400°C with flow rate of 20 $mLmin^{-1}$, ramp rate of 10°$Cmin^{-1}$ and holding at 400°C for 30 min. The hydrogen consumption as a function of linearity temperature was monitored by TCD and reported as a reduction profile.

3.2.7 X-ray Diffractometer (XRD)

All synthesized photocatalysts powder prepared by complex-precipitation and wet impregnation were subjected to XRD (Bruker D8 Advance) with CuKα radiation (40 kV, 40 mA) at 2θ angles from 10° to 80°, with a scan speed of 4°min^{-1}. An adequate amount of powder samples was even-out on a disc using a glass slide and was placed on the stage for scanning.

3.3 PHOTOCATALYTIC ACTIVITY

Photocatalytic reaction was performed at room temperature using a multiport (40 mL) each reactor. A 500 W halogen lamp was used as the light source, which was positioned on top of the multireaction port at 15 cm distance to the lamp with the intensity of 368 Wm^{-2}. Approximately 0.1 g of each sample was dispersed in 8 mL of distilled water with the addition of 0.5 mL of methanol. A comparison study was carried out without the addition of methanol. The gas evolved was collected using a water displacement apparatus and monitored over a period of 1 hour. Figure 3.2 shows the setup for the reaction. The gaseous products were analyzed using TCD-MS with N_2 as the carrier gas flowing at 20 $mLmin^{-1}$. As for the aqueous portion, 2-3 drops of Schiff reagent was added into the solution to determine the presence of formaldehyde.

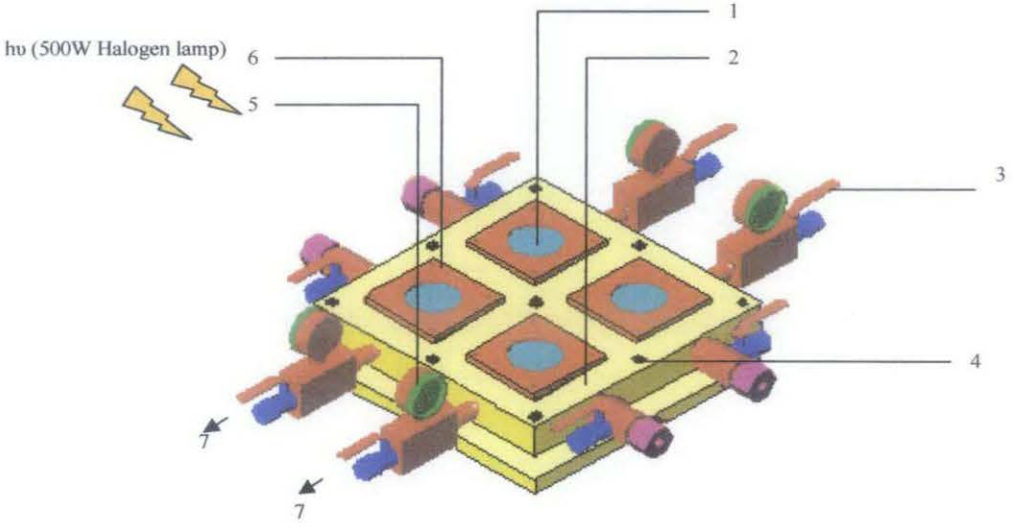

Key:

1. Quartz window	3. One way valve	5. Gauge pressure	7. To water displacement unit
2. Acrylic board	4. Screw	6. Metal plate	

Figure 3.2 Photocatalytic reaction set up.

CHAPTER 4

RESULTS AND DISCUSSION

4.1 ACTIVATION OF PHOTOCATALYST

The desired calcination temperatures of the prepared Cu/TiO_2 photocatalysts were determined from the thermal gravimetric analysis. Prior to calcination, this step was conducted to monitor the decomposition temperature of the photocatalysts, at which temperature it begins to decompose and the temperature range where the uncalcined catalyst has achieved thermal stability. The optimum calcination temperatures were then determined.

4.1.1 Thermal Gravimetric Analysis (TGA) of Uncalcined Cu/TiO_2 Photocatalyst

To investigate the thermal behaviour of the uncalcined Cu/TiO_2 photocatalysts, a thermal gravimetric analysis (TGA) was performed. Results from TG analysis of the Cu/TiO_2 catalyst prepared by precipitation and wet impregnation method were shown in Figure 4.1. The TG thermogram of the photocatalysts prepared by copper complex-precipitation method (10CuGT) showed a slow weight loss from room temperature to 150°C, at which an accelerated loss of weight occurred until 350°C and a slight weight gain around 400°C. The first weight loss step occurred between 30°C to 150°C depicts the evaporation of the physically adsorbed water (Haruhiko and Tomoko, 1982; Sun *et al.*, 2005) took place for copper supported on TiO_2 (Figure 4.1). The intense weight loss (Figure 4.1) between 150°C to 350°C, corresponding to a total of 8 wt% weight loss depicts the two possible

decomposition compounds that is glycerol (Binlin *et al.*, 2009) and copper-glycerol hydroxides to CuO (Li *et al.*, 2006; Marc *et al.*, 1996) (Equation 4.1).

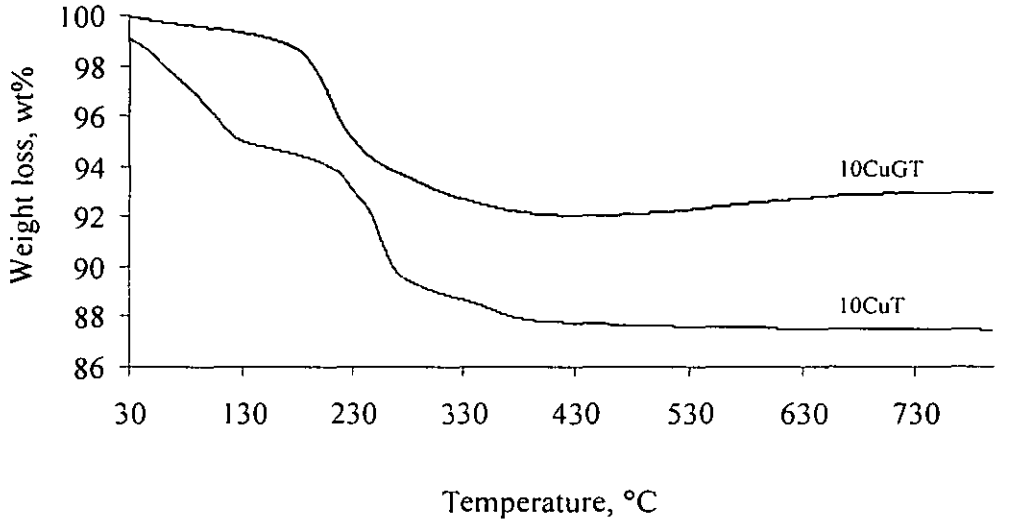

Figure 4.1 Thermal decomposition of uncalcined Cu/TiO_2 catalyst using complex-precipitation and wet impregnation methods.

$$Cu(OH)_x(C_3H_6O_3)_z \xrightarrow[\Delta]{} CuO_{(s)} + H_2O_{(g)} + CO_{2\ (g)} \quad (4.1)$$

$$Cu(NO_3)_2 \xrightarrow[\Delta]{} CuO_{(s)} + 2NO_{2\ (g)} + O_{2\ (g)} \quad (4.2)$$

As for Cu/TiO_2 prepared by wet impregnation, the TG curve was slightly different compared to the complex-precipitation. Two sharp decomposition curves were observed in Figure 4.1. The weight loss of 4 wt% at the first decomposition curve from 30°C to 110°C was attribute to the evaporation of water molecule contained or trapped in the sample (Wu and Chih, 2001) and the second weight loss of 5.5 wt% from 110°C to 270°C as well as a slight weight loss of 2 wt% from 270°C to 370°C showed the decomposition of nitrate salts (Equation 4.2). The total weight loss was calculated to be 11.5 wt%.

A steady horizontal line indicates no further weight loss or weight gain. The TG curves were used to obtain information about the optimum calcination temperature of the samples (Moura *et al.*, 2005). From the TG curves, the estimated minimum calcination temperature of the photocatalysts was 400°C onwards.

4.1.2 Fourier Transform Infrared (FTIR) Spectra of Cu/TiO_2 Photocatalyst

Figure 4.2 showed the FTIR transmission spectra of photocatalysts calcined at 300°C, 400°C and 500°C for 30 min. For comparison purpose, the FTIR spectrum for glycerol, CuGT and CuT precursors are shown in Appendix E. For all the spectra shown in Figure 4.2, the absorption peak around 1600 cm^{-1} and 3400 cm^{-1} were attributed to the O-H bending and stretching, respectively (Li *et al.*, 2005). The broad band observed between 400–900 cm^{-1} correspond to the Ti-O stretching vibrations (Appendix E) (Linacero *et al.*, 2006; Porkodi and Arokiamary, 2007; Yan *et al.*, 2004). From the FTIR spectrum in Figure 4.2, the presence of the NO_3^- group at 872 cm^{-1} and 1384 cm^{-1} (Niu *et al.*, 2006) are unable to distinguish due to the overlapping of the TiO_2 anatase peak. Furthermore, the weak absorption band appears at 3000 cm^{-1} to 3200 cm^{-1} for CuGT samples are corresponded to the C-H region, contributed by the glycerol fragments in which it has not completely eliminated during calcination (Nakamoto, 1997). Hence, it is believed that the calcination duration took place for 30 min were insufficient to remove all the nitrate salts as well as carbon components from glycerol present during preparation.

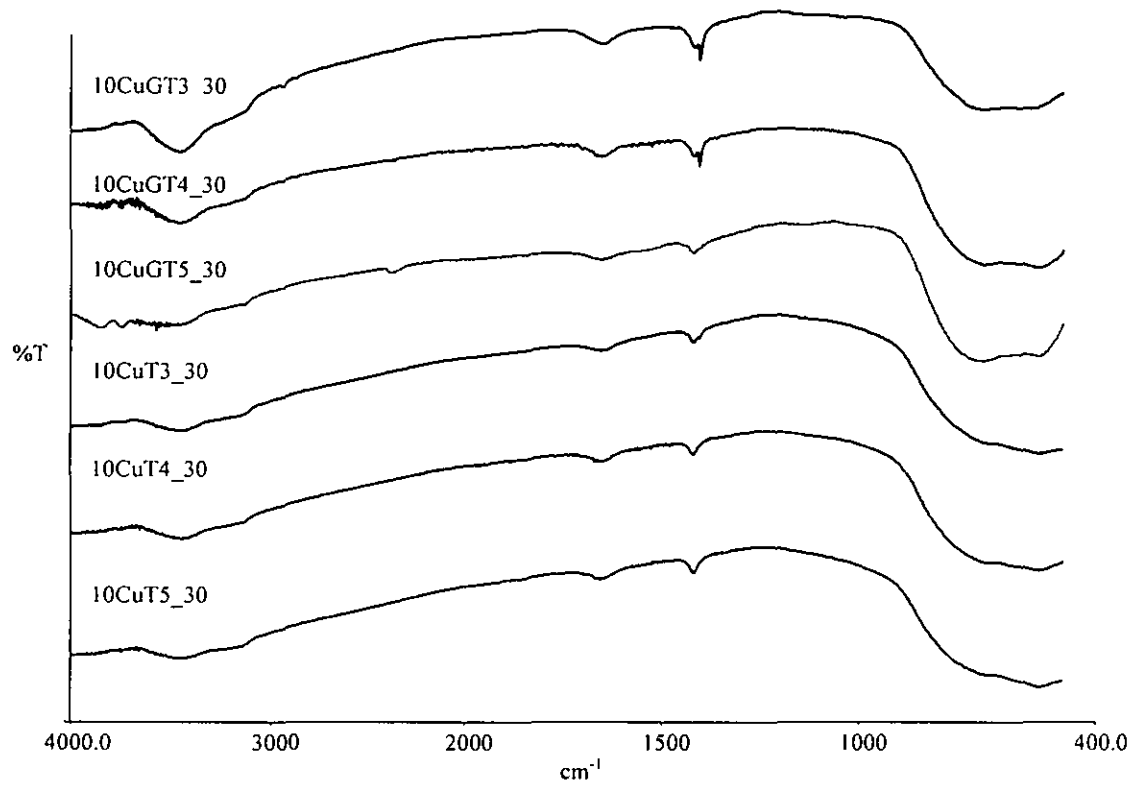

Figure 4.2 The FTIR spectra of Cu/TiO_2 catalyst prepared using complex-precipitation and wet impregnation methods.

4.2 PHOTOCATALYTIC ACTIVITY FOR Cu/TiO_2 PHOTOCATALYST

Numerous studies have shown that the hydrogen yield strongly depends on the calcination temperature as a treatment method to control the crystalinity, S_{BET} and photocatalytic activity materials (Singto *et al.*, 2005). In this study, the photocatalytic activities of Cu/TiO_2 with metal loading of 2, 5, 10 and 15 wt% were investigated in terms of the dependence of calcination temperatures and the effect of copper loading. The photoactivity experiments were carried out on the water-methanol systems prepared by complex-precipitation and wet impregnation. However, only selected photocatalysts prepared from both methods were sent for characterization to determine their properties.

Figure 4.3 displays the photocatalytic activity of Cu/TiO_2 for both preparation methods. The amount of gas evolved increased with increasing Cu loading from 2 wt% to 10 wt%.

However, further increase in metal loading (15 wt%) reduced the amount of gas produced. In order to determine the optimum Cu loading, photocatalysts with two different loading 9 wt% and 11 wt% were prepared for both preparation methods and screened for photoactivity. The results showed that the optimum Cu loading is 10 wt% for both methods. Based on Figure 4.3, photocatalysts prepared by complex-precipitation method showed better photoactivity compared to those by wet impregnation for all metal loading.

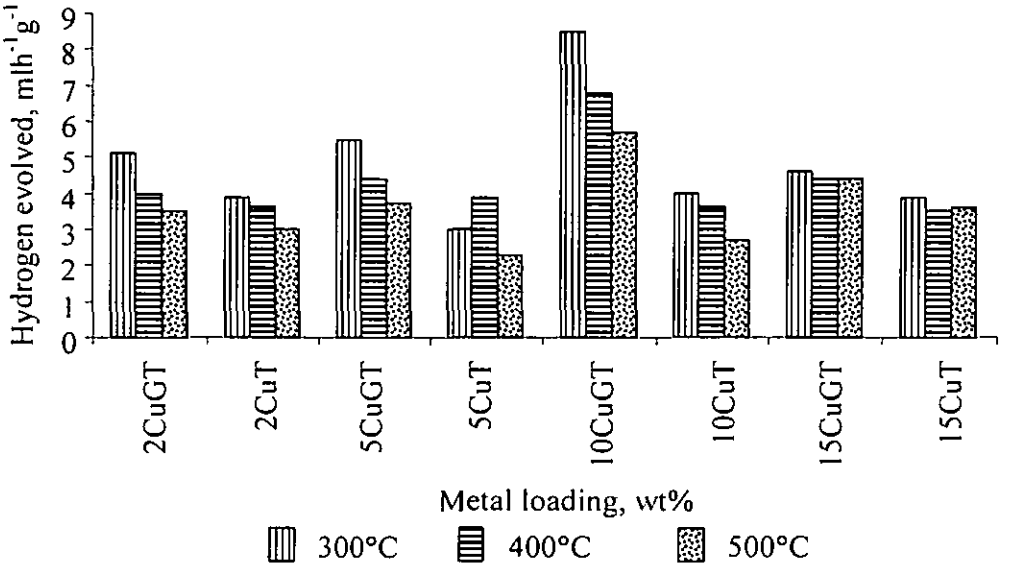

Figure 4.3 Comparisons of the Cu/TiO_2 photocatalytic activity with various calcination temperatures.

The highest amount of gas evolved obtained from catalysts prepared by complex-precipitation was 10CuGT3_30 (8.5 $mLh^{-1}g^{-1}$) followed by 10CuGT4_30 (6.8 $mLh^{-1}g^{-1}$) and 10CuGT5_30 (5.7 $mLh^{-1}g^{-1}$). On the other hand, the highest gas evolution for those prepared by wet impregnation was 10CuT3_30 (4.0 $mLh^{-1}g^{-1}$) followed by 10CuT4_30 (3.6 $mLh^{-1}g^{-1}$) and 10CuT5_30 (2.7 $mLh^{-1}g^{-1}$). Comparisons of photocatalytic activity were also study without the addition of methanol as control experiments and the results for complex-precipitation are 4.5 $mLh^{-1}g^{-1}$, 3.2 $mLh^{-1}g^{-1}$ and 2.5 $mLh^{-1}g^{-1}$ for 10CuGT3_30, 10CuGT4_30 and 10CuGT5_30, respectively. As for wet impregnation the amount of gas obtained was 3.0 $mLh^{-1}g^{-1}$, 2.8 $mLh^{-1}g^{-1}$ and 2.0 $mLh^{-1}g^{-1}$ for

10CuT3_30, 10CuT4_30 and 10CuT5_30, respectively. In the case of titania P25, the photocatalytic activity exhibit only 2.5 $mLh^{-1}g^{-1}$. The photocatalytic performance was found to be lower than the water-methanol system. Table 4.1 summarizes the comparison of gas production from catalysts prepared by both methods.

Table 4.1 Comparison of gas production with and without methanol as scavenger.

Photocatalysts	H_2 evolution, $mLh^{-1}g^{-1}$	
	Addition of 0.5 mL MeOH	No addition of MeOH
10CuGT3_30	8.5	4.5
10CuGT4_30	6.8	3.2
10CuGT5_30	5.7	2.5
10CuT3_30	4.0	3.0
10CuT4_30	3.6	2.8
10CuT5_30	2.7	2.0
TiO_2	not determined	2.5

In this study the photocatalytic performance is influenced by the amount of metal loading, calcination temperatures and the preparation methods. The increase in metal loading enhances the photocatalytic activity by effectively inhibit the electron-hole recombination in TiO_2. As mentioned earlier, the H_2 yield increased initially with increasing Cu content of the catalyst, reached a maximum and then started to decrease once the Cu content was increased beyond 11 wt%. The reason given for this trend in reaction behavior is that the deposition of small amounts of Cu is indispensable for the removal of photogenerated electrons from TiO_2 (Gratian *et al.*, 1995). However, as more and more Cu is added to the TiO_2 surface beyond a certain optimum value (11 wt%), blockage of the photosensitive TiO_2 surface occurs. According to Yuan *et al.* (2006), this will eventually limits the light penetration reaching the support and decrease the surface concentration of electrons and holes pairs available for reaction (Behnajady *et al.*, 2008; Carp *et al.*, 2004) which consequently lowered the TiO_2 photoactivity. Another reason is that, at higher Cu loading, the deposited Cu particles may act as recombination centers for photogenerated electron and holes (Dhanalakshmi *et al.*, 2001; Gratian *et al.*, 1995). In addition, excessive Cu

loading will results in the growth and agglomeration of the Cu particles on TiO_2 surface leading to lower photocatalytic activity (Dhanalakshmi *et al.*, 2001; Yi *et al.*, 2008).

In terms of calcination temperature, the photocatalytic activities of 10CuGT and 10CuT samples significantly decrease with the increase in calcination temperature from 300°C to 500°C. The significant decrease in the photocatalytic activity observed especially for wet impregnation samples calcined at temperature higher than 300°C where the surface areas for these samples were reduced from 63.83 m^2g^{-1} (300°C) to 35.44 m^2g^{-1} (500°C). This could be attributed to the growth and agglomeration of the particles (reducing particles surface area) as proposed by Singto *et al.* (2005) This phenomenon will eventually weakens the interaction of CuO-TiO_2 resulting in lower photocatalytic activity (Bandara *et al.*, 2005; Yasomanee and Bandara, 2008).

In addition, the higher calcination temperatures not only led to formation of larger particle size but results in a longer electron transfer distance and higher rate of "electron-hole pair recombination" thus reducing the hydrogen evolution (Yi *et al.*, 2008) for both samples calcined at 500°C. Furthermore, the low activity shown by the wet impregnation samples calcined at 400°C and 500°C compared to 300°C could be due to its negative effect from low surface area, which is not compensated by the higher degree of CuO crystallinity as shown in XRD (Figure 4.9)

The effect of transition metal incorporation such as Cu resulted in the improvement of the photocatalytic activity compared to TiO_2 only. According to Sadhana *et al.* (2007), the benefit of transition metal doping is in its higher capability to trap electrons or inhibiting electron hole recombination during illumination. The incorporation of these transition metal ions, as mentioned earlier could effectively enhance the light absorption spectrum of the photocatalysts to the visible region (Masakazu, 1997; Yi *et al.*, 2008). The improvement of the photocatalyst activity for Cu/TiO_2 may be due to the incorporation of Cu^{2+} that it is a coloured ion and thus acts as a chromophore, which absorbs light in the visible range (Sadhana *et al.*, 2007). The ability of the photocatalysts which absorbs

longer wavelength was proven by the DR-UV-Vis spectra (Figure 4.5) where the absorption edges were shifted to longer wavelength.

For photocatalytic mechanism for H_2 evolution in the presence of methanol (as hole scavenger), the reduction of H_2O molecule and the removal of hole (h^+) proceed simultaneously (Figure 4.4). In this manner, CuO serves as an electron (e^-) trapper and suppresses the recombination of holes and electrons. In order to achieve efficient H_2 evolution, the photogenerated electrons, upon band gap excitation, must be rapidly injected from the valence band (VB) to the conduction band (CB) of TiO_2 photocatalyst and subsequently to the metal oxide (CuO), aqueous methanol solution was then used to stabilize the accompanying holes to prevent the recombination (Thammanoon *et al.*, 2005). The hydrogen evolution from the photocatalytic activity was confirmed by mass spectroscopy.

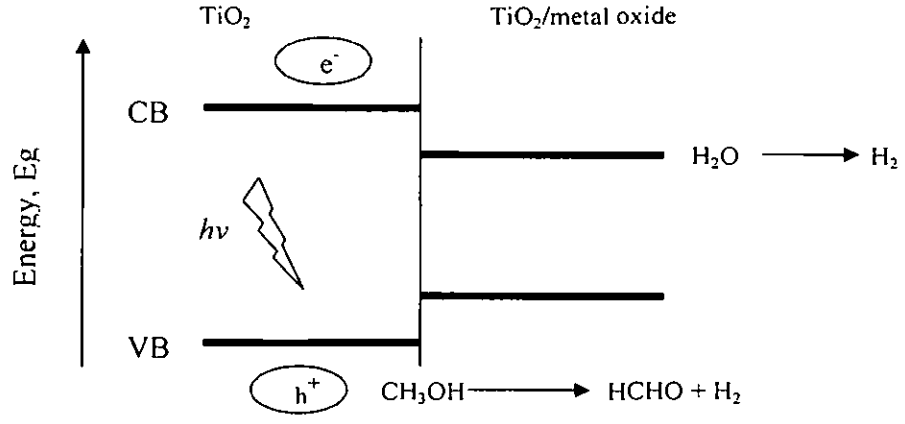

Figure 4.4 Schematic diagram for the mechanism of photocatalytic H_2 production (Bandara *et al.*, 2005).

4.3 PHOTOCATALYST CHARACTERIZATION

4.3.1 Field Emission Scanning Electron Microscope (FE-SEM) of Cu/TiO_2 Photocatalyst

Scanning electron micrographs were taken for all samples. Figure 4.5 (a)–(f) showed micrographs of copper supported TiO_2 and Figure 4.5 (g) showed the morphology of TiO_2 only. The particle structures were found to be irregular in all the samples and the spherical particles with wrinkled surface was identified to be TiO_2 (Figure 4.5 (g)). The sizes of the particles were around 20-100 nm in size for all the samples (Figure 4.5 (a)-(g)). The irregularities in the particle structure might have occurred during the grinding of the samples. The FE-SEM indicates that the particles were very small for all samples. The morphologies of photocatalysts prepared by complex-precipitation method as shown in Figure 4.5 (a)-(c) are spherical. Agglomeration became more obvious for 10CuGT5_30 (Figure 4.5 (c)) which may be caused by sintering effect as a result of increase in calcination temperature. From the results displayed in Figure 4.5 (a)-(c), the CuO clusters were not noticeable for all 10CuGT samples. One of the reason that explains this phenomena is the high dispersion degree that could be contributed by the addition of glycerol as a ligand which helps to prohibit the aggregation of the metal particle and favor the formation of highly dispersed metal oxides onto the support when the ligand starts to decompose during calcination (Amit and Sharma, 2002; Li *et al.*, 2006). The rod like and platelet shaped morphology (shown in arrow) of the 10CuT calcined at 300°C, 400°C and 500°C showed the CuO clusters deposited on the surface of the TiO_2. Hence, an elemental analysis was carried out to confirm this impurity. However, the EDX analysis for 10CuT3_30 showed an unclear view of the Cu element (shown in arrow) due to charging effect (Appendix C).

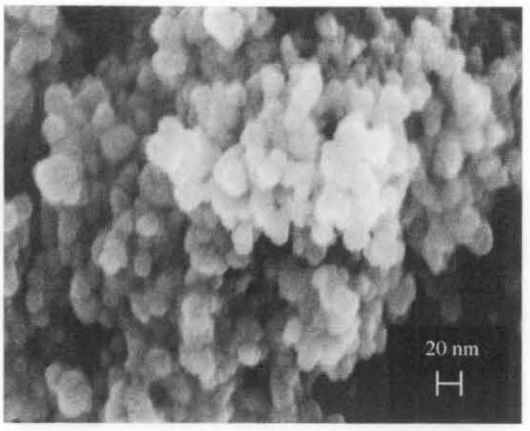

(a) 10CuGT3_30 100KX

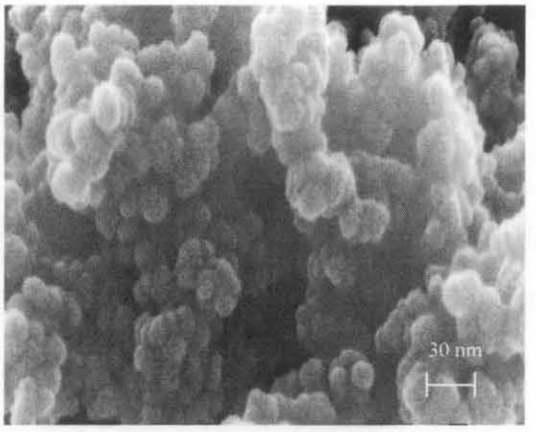

(b) 10CuGT4_30 100KX

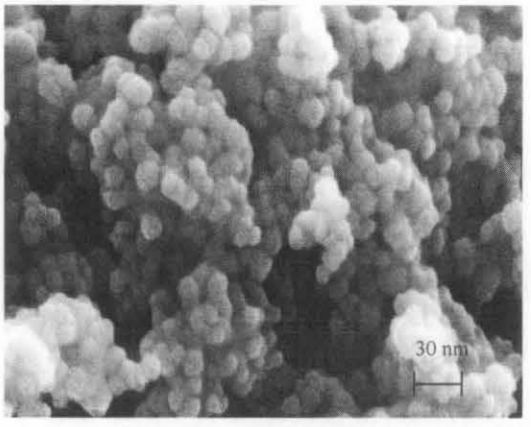

(c) 10CuGT5_30 100KX

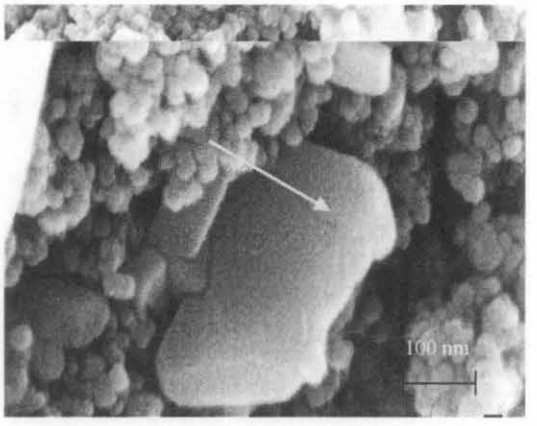

(d) 10CuT3_30 100KX

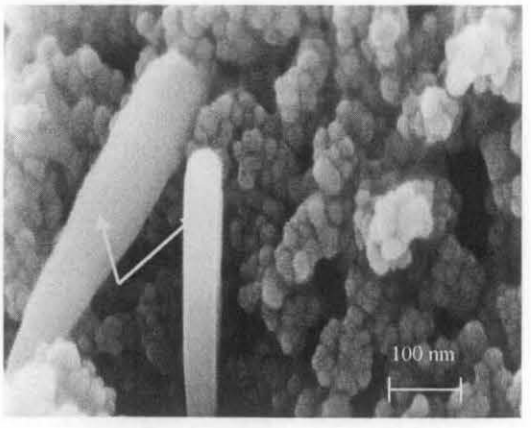

(e)10CuT4_30 100KX

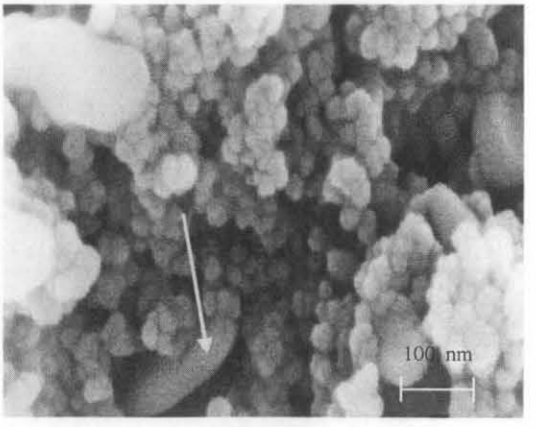

(f)10CuT5_30 100KX

Figure 4.5 The FE-SEM micrographs of the Cu/TiO_2 and TiO_2 photocatalyst.

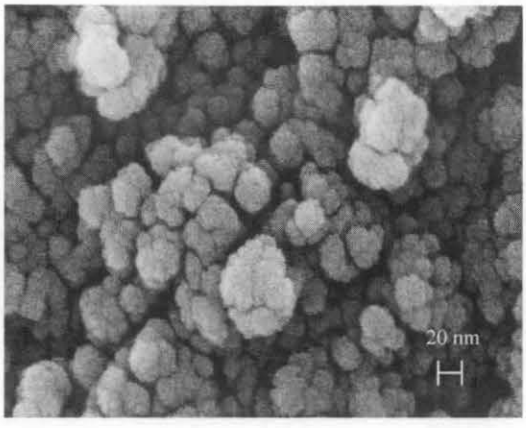

(g) TiO_2 100KX

Figure 4.5 The FE-SEM micrographs of the Cu/TiO_2 and TiO_2 photocatalyst (continued).

4.3.2 Surface Area of Cu/TiO_2 Photocatalyst

The BET surface area of the calcined samples for Cu/TiO_2 and TiO_2 photocatalyst are shown in Table 4.2. The N_2 adsorption-desorption isotherm for all the Cu photocatalysts prepared by complex-precipitation and wet impregnation showed IUPAC of type IV pattern with H1 hysteresis loop which indicates mesoporosity (Rahimnejad *et al.*, 2008). According to Leofanti *et al.* (1998), the H1 hysteresis loop is characteristic of solids consisting of particles crossed by nearly cylindrical channels or made by aggregates (consolidated) or agglomerates (unconsolidated) of spheroidal particles. TiO_2 displayed type III pattern, which is typically ascribed to non-porous products with weak interactions between the adsorbent and the adsorbate (Appendix D). The surface area of the photocatalysts was found to decrease slightly due to the increase in calcination temperature.

As observed in Table 4.2, the higher surface area was obtained for 10CuT3_30 (63.83 m^2g^{-1}) compared to 10CuGT3_30 (42.20 m^2g^{-1}) was mainly contributed by surface area of the copper oxide deposited on TiO_2 surface as evidence in the FE-SEM micrograph (Figure 4.5 (d)). According to Colon *et al.* (2006), the higher surface value might be attributed to the increased in surface porosity due to the elimination of nitrate from Cu

during calcination at temperature lower than 400°C. However, the surface area obtained for 10CuT3_30 was non-agreeable with Colon *et al.* (2006) as there were some traces of nitrate observed in FTIR (Figure 4.2). Although 10CuT3_30 gave the highest surface area, in terms of photocatalytic activity, it displayed lower performance compared to 10CuGT3_30 as depicted in Figure 4.3. This is because CuO alone could not be used to generate H_2 from water due to the less negative conduction band edge compared to the reduction potential of water (Dong *et al.*, 2004). This could be one of the reasons that explain the lower photocatalytic activity obtained by 10CuT3_30.

Table 4.2 Surface area of the photocatalysts.

Photocatalysts	Surface area, m^2g^{-1}
TiO_2	53.44
10CuGT3_30	42.20
10CuGT4_30	45.13
10CuGT5_30	42.38
10CuT3_30	63.83
10CuT4_30	42.69
10CuT5_30	35.44

4.3.3 Diffuse Reflectance UV Visible Spectra (DR-UV-Vis) Spectra of Cu/TiO_2, Photocatalyst

The DR-UV-Vis spectra of all the Cu/TiO_2 and TiO_2 samples are presented in Figure 4.6. The spectrum of TiO_2 showed the absorption peak at 388 nm similar to that observed by Anpo and Takeuchi, (2003) which is in the UV region. The presence of this strong absorption band at low wavelength in the spectra 388 nm indicates the Ti species as tetrahedral Ti^{4+}. This absorption band is generally associated with the electronic excitation of the O 2p electron in valence band to the conduction band Ti 3d band (Fuerte *et al.*, 2002; Thammanoon *et al.*, 2005). Surface modification of TiO_2 with CuO significantly affects the absorption properties as shown in Figure 4.6. It can be seen that the diffuse reflectance spectra of Cu/TiO_2 photocatalysts are different from the bare TiO_2.

It is noticeable that the incorporation of 10 wt% copper onto TiO_2, showed a considerable shift towards the visible range (400 to 800 nm) for all samples prepared by both methods. This observation may be attributed to the presence of impurities and defect site due to the incorporation of copper species (Junya *et al.*, 2005).

According to Colon *et al.* (2006), the band at 210-270 nm would indicate the O^{2-} (2p)$\rightarrow Cu^{2+}$ (3d) ligand to metal charge transfer transition, where Cu ions occupy isolated sites on the support. A broad band between 400-600 nm attributed to the presence of Cu^{+} clusters in partially reduced CuO matrix, as well as $(Cu\text{-}O\text{-}Cu)^{2+}$ clusters. The absorption band at 600-800 nm indicates the crystalline and bulk CuO in octahedral symmetry (Colon *et al.*, 2006). The incorporation of copper ion could instigate the absorption band in visible or near-infrared range which promotes the photocatalytic activity of 10CuGT3_30 and 10CuT3_30 as shown by the absorption spectra (Figure 4.6). Thus, it was found that doping transition metal such as copper was effective for visible light response (Akihiko *et al.*, 2007; Zou and Arakawa, 2003) and is playing a significant role in enhancing hydrogen evolution (Sadhana *et al.*, 2007).

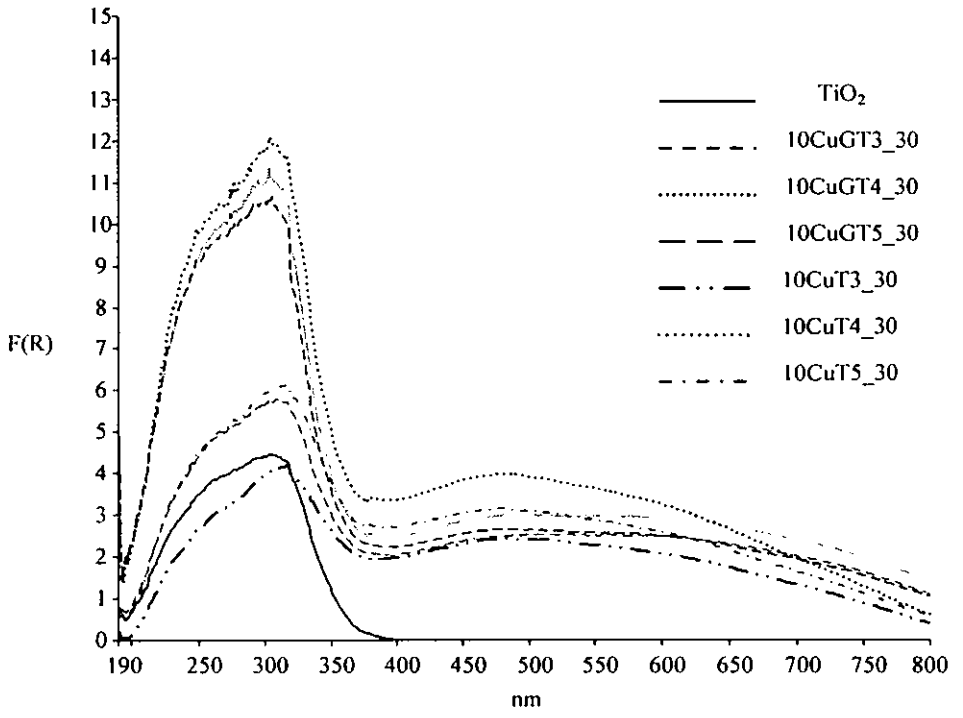

Figure 4.6 The DR-UV-Vis spectra of TiO_2 and Cu/TiO_2 prepared using complex-precipitation and wet impregnation methods.

The band gap calculation for all samples were estimated by using the Tauc's plot $[F(R).hv]^{1/2}$ vs hv, where $F(R) = (1-R)^2/(2R)$ is the formula of Kubelka-Munk and hv is the photon energy (Chiang *et al.*, 2002; Diamandescu *et al.*, 2008; Murphy, 2007; Yuan *et al.*, 2006). The band gap energies were deduced from the intersection of the Tauc's region extrapolation with the photon energy axis (Figure 4.7). The calculated values of band gap energy are given in Table 4.3. The data is compared with the amount of H_2 evolved during reaction. The biggest reduction in band gap energy observed for 10CuT3_30 does not display the best performance compared to the other catalysts. In order for enhanced photocatalytic activity, good interaction of CuO with TiO_2 is required. The small band gap obtained for 10CuT3_30 (2.4 eV) could be related to the big CuO particles without interaction with TiO_2 as observed in the FE-SEM micrographs (Figure 4.5 (d)-(f)).

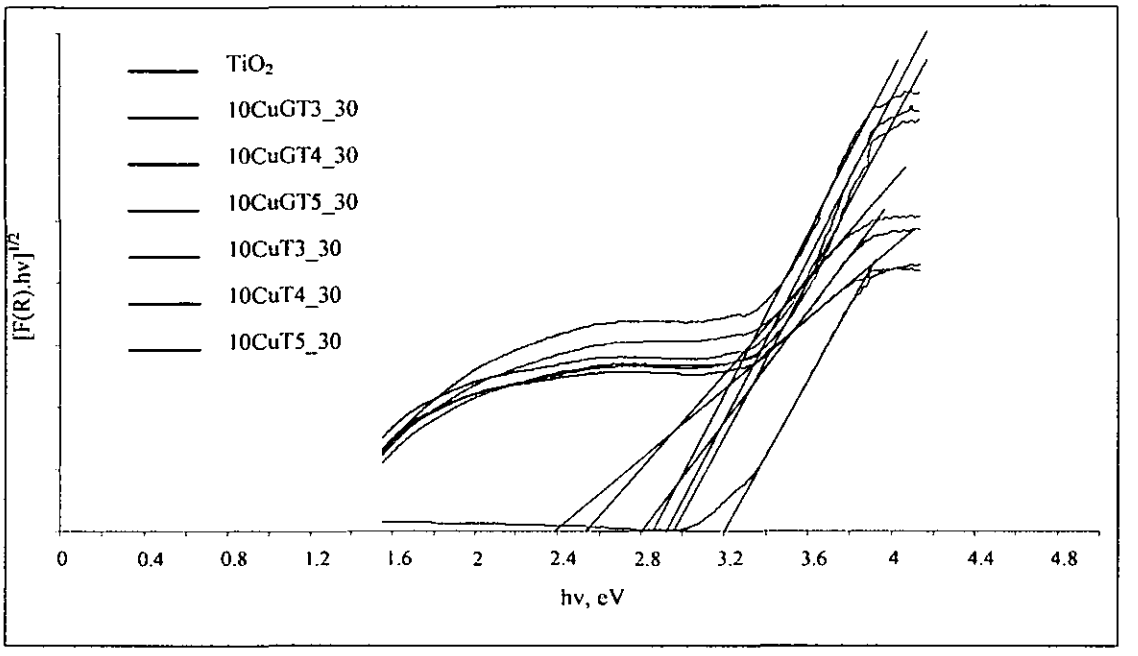

Figure 4.7 Plot of transformed Kubelka-Munk functions $[F(R).hv]^{1/2}$ vs hv for Cu/TiO_2 and pure TiO_2 samples to estimate band gap energies.

Table 4.3 Summary of the band gap energies estimated from UV-Vis data on the prepared samples compared to Degussa P25.

Photocatalyst	Band gap energy, eV
TiO_2 (Degussa P25)	3.20
10CuGT3_30	2.93
10CuGT4_30	2.91
10CuGT5_30	2.75
10CuT3_30	2.40
10CuT4_30	2.85
10CuT5_30	2.58

4.3.4 Temperature Programmed Reduction (TPR) of Cu/TiO_2 Photocatalyst

Figure 4.8 (a) and (b) displayed the TPR profiles of calcined Cu/TiO_2 prepared by complex-precipitation and wet impregnation, respectively. Temperature Programmed

Reduction (TPR) is used to characterize the Cu/TiO_2 photocatalyst with respect to the type of copper species present and the degree of interaction with TiO_2 support for various calcination temperatures.

Obviously, the TPR profile for photocatalysts prepared by complex-precipitation (Figure 4.8 (a)) displayed major peaks as well as shoulders for samples calcined at 300°C, 400°C and 500°C. The shoulders which have lower reduction temperature indicate the reduction of small CuO species having less interaction with the support. As the calcination temperature increases, the intensity of these shoulders became less noticeable. In addition, the peaks positions were shifted to higher reduction temperature. The shift in reduction temperature of these samples can be explained by the increase in calcination temperatures which causes the growth and agglomeration of the particles. This could lead to the presence of less accessible and lower reducibility of CuO species in the samples which lessen the hydrogen consumed during the reduction process (Cordoba *et al.*, 1998). Therefore, the species that could be present at higher reduction temperature around 251°C, 264°C and 285°C may be due to the bulk CuO (Albin *et al.*, 2005; Boccuzzi *et al.*, 1997; Mile *et al.*, 1990) having strong metal-support interaction (SMSI) (Feg *et al.*, 1998; Larsson *et al.*, 1996).

As for the wet impregnation, Figure 4.8 (b) the reduction profile showed two reduction peaks for Cu-Ti-O calcined at 400°C and 500°C but a single peak for calcination at 300°C (Figure 4.8 (b)) with reduction temperature of 233°C (Table 4.4). The Cu/TiO_2 which have lower reduction temperature peak between 169°C and 172°C (Table 4.4) may be ascribed to the reduction of small metal oxide particles having little or no interaction with the support (Liu *et al.*, 2006; Zhu *et al.*, 2006). According to Albin *et al.* (2005) and Marta *et al.* (2002), the lower reduction peaks (169°C and 172°C) are associated to the presence of other copper species. This species could be the $Cu^{2+} \rightarrow Cu^{+}$ reduction and the higher reduction peak (233°C and 241°C) is attributed to, $Cu^{+} \rightarrow Cu^{0}$ reduction. The reduced species obtained is agreeable with the observation from DR-UV-Vis spectra shown in Figure 4.6.

TPR profile of all the samples, together with XRD results gave consistency in the type of species being reduced during reduction. XRD results showed that the prepared Cu/TiO_2 had only XRD peaks corresponding to CuO (Figure 4.9). The increasing intensity of the CuO crystallite peaks observed in XRD is in agreement with the reduction of bulk CuO at higher temperature (Table 4.4).

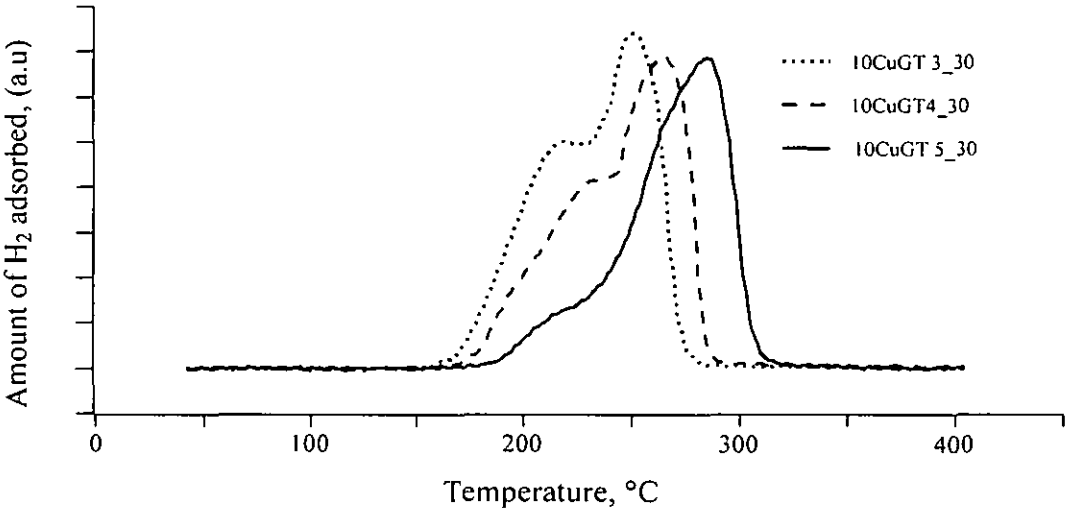

Figure 4.8 (a) TPR profile of 10 wt% copper loading with different calcination temperatures using complex-precipitation method.

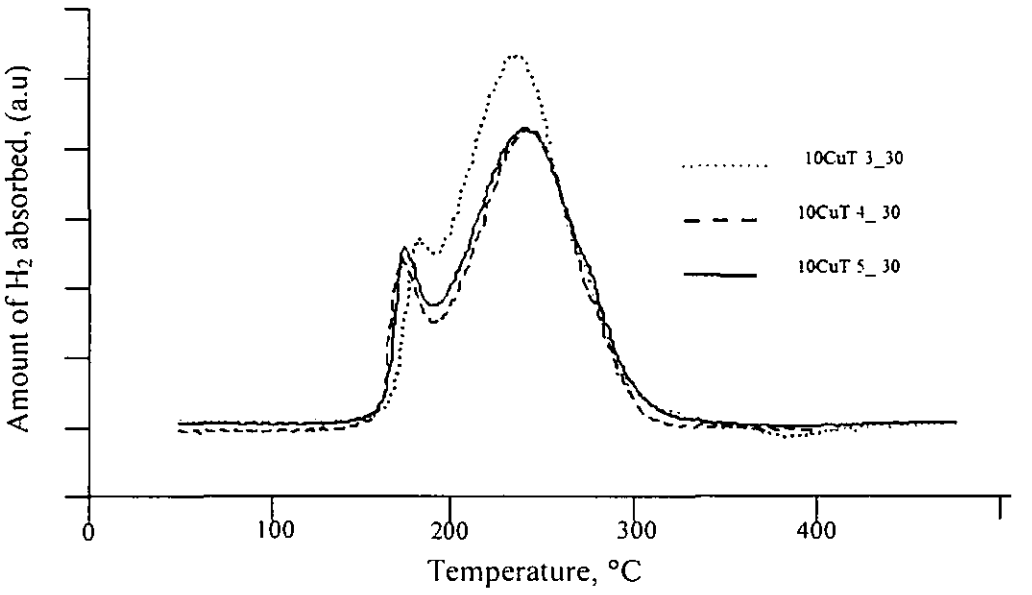

Figure 4.8 (b) TPR profile of 10 wt% copper loading with different calcination temperatures prepared using wet impregnation method.

Table 4.4 Summary of the hydrogen consumption and the reduction temperature of the samples.

Samples	Reduction peaks, T(°C)	Amount of H_2 consumed, µmol/g
10CuGT3_30	251	1429
10CuGT4_30	264	1309
10CuGT5_30	285	1210
10CuT3_30	233	1322
10CuT 4_30	172, 241	1165
10CuT 5_30	169, 241	1203

4.3.5 X-ray Diffractometer (XRD) of Cu/TiO_2 Photocatalyst

The XRD diffractogram for photocatalysts prepared using complex-precipitation and wet impregnation with calcination temperature of 300°C are displayed in Figure 4.9 (b) and (c). The diffraction pattern of undoped TiO_2 was also included in Figure 4.9 (a) for comparison while the remaining of the XRD diffractograms is displayed in Appendix E.

It is observed that the TiO_2 support for all samples is still in the anatase phase and the TiO_2 peak position still remains unchanged even with calcination temperature up to 500°C.

The diffraction peaks at 2θ of about 25.34°, 337.9°, 47.8°, 53.8° and 55.0° shown in Figure 4.9 represent the indices of (101), (004), (200), (105) and (211) phase plane, which were confirmed to crystalline structure of TiO_2 anatase (Hedge *et al.*, 1997; Kaifu *et al.*, 2006; Kenning *et al.*, 2003; Thammanoon *et al.*, 2005; Yong *et al.*, 2006) and 2θ =27.42° exhibits in all samples correspond to the rutile phase (Slamet *et al.*, 2005).

The CuO (tenorite) diffraction peak appeared near 2θ =35.6° and 38.73° for all samples especially for samples prepared using wet impregnation (Figure 4.9 (c)) (Albin *et al.*, 2005; Hyung and Misook, 2007; Marc *et al.*, 1996). As revealed in Appendix E, the CuO peak showed an increased intensity with the rising calcination temperature from 300°C to 500°C for all samples. The result obtained in this study was similar to Bandara *et al.* (2005). This indicates that the catalysts have higher degree of crystallinity and relatively larger grain size (Gen *et al.*, 2006; Valdeilson *et al.*, 2007). Meanwhile, the crystalline peak of CuO was less noticeable for samples prepared using complex-precipitation method compared to the wet impregnation method (Appendix E). Preparation of photocatalyst by complex-precipitation did not reveal any intense crystalline phase of CuO as evidence by the FE-SEM results (Figure 4.5 (a)–(c)). This indicates that if part of the Cu exists in the form of CuO clusters, these are not large enough to be detectable by XRD (Cordoba *et al.*, 1998). This phenomenon suggested that the complex-precipitation method stabilizes the CuO phase in a dispersed state (Chiang *et al.*, 2002; Gen *et al.*, 2006; Slamet *et al.*, 2005).

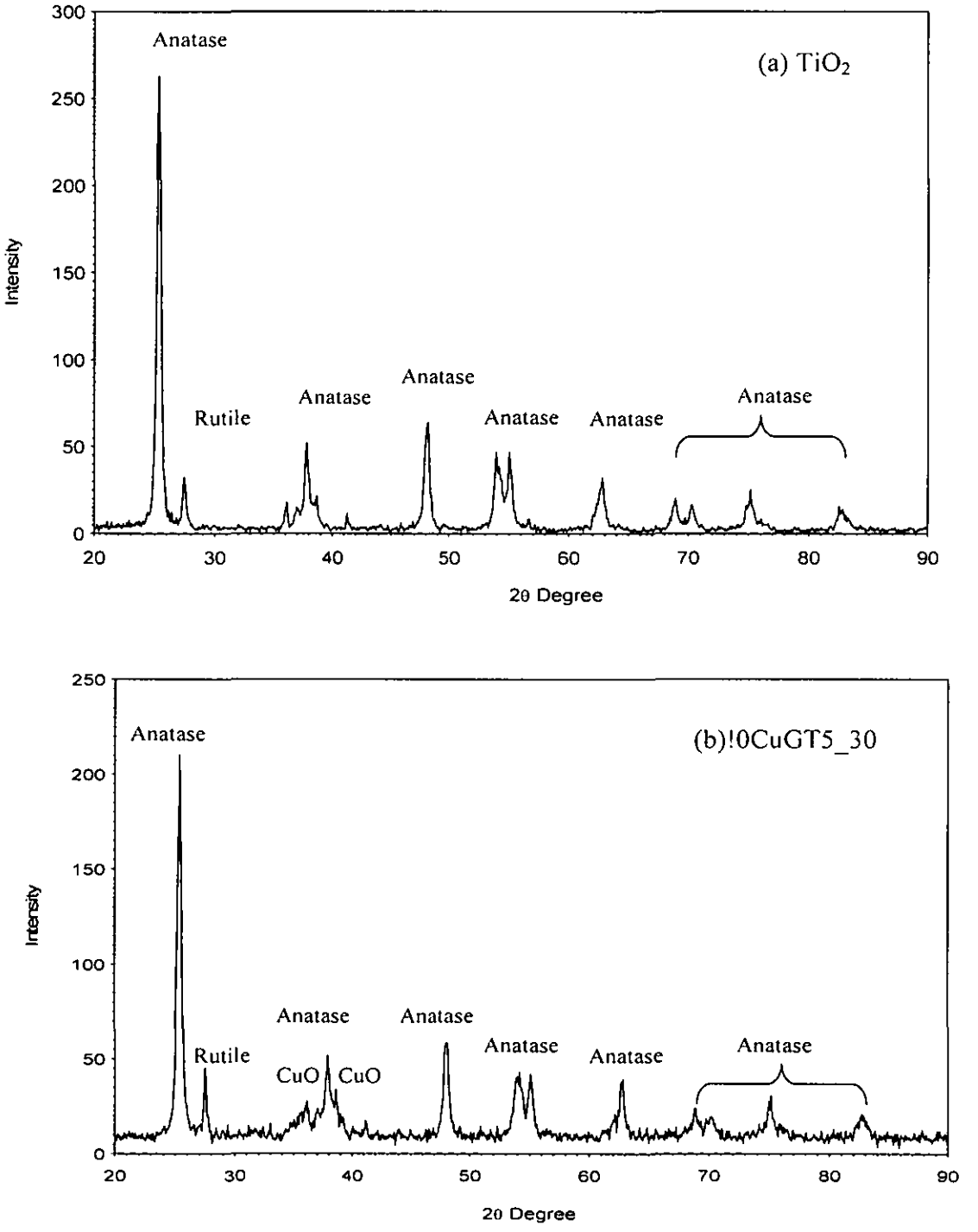

Figure 4.9 Comparison of XRD diffractograms for (a) TiO_2, (b) 10CuGT5_30 and (c) 10CuT5_30.

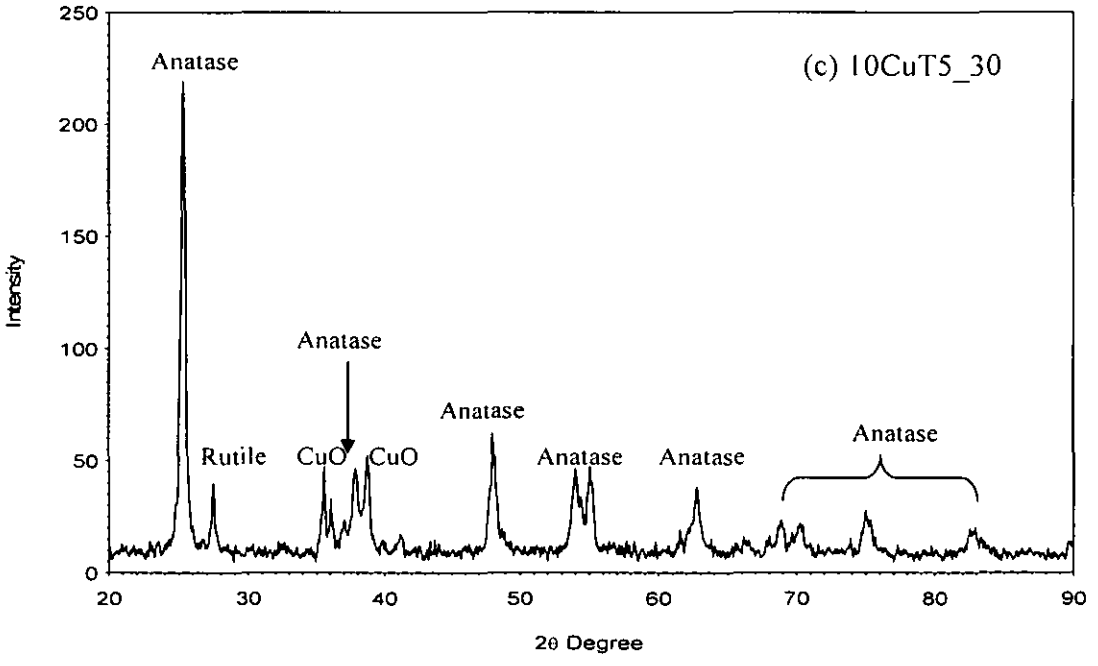

Figure 4.9 Comparison of XRD diffractograms for (a) TiO_2, (b) 10CuGT5_30 and (c) 10CuT5_30 (continued).

CHAPTER 5

CONCLUSIONS AND RECOMMENDATIONS

5.1 Conclusions

Based on the findings as reported in Chapter 4, a number of conclusions were made with regards to its preparations and factors that govern the photocatalytic activity. Firstly, the heat treatment was found to be a crucial step in the preparation process, as it has important implications on the photocatalytic activity. The photocatalytic activity of the prepared Cu/TiO_2 photocatalysts was found to decrease with an increase in the heat treatment (Table 5.1). The low photocatalytic activity was explained in terms of the agglomeration of particles during calcination at high temperatures (400°C and 500°C) which led to the reduction in the surface area of the samples.

Secondly, one of the objectives of this study was to develop photocatalyst which is able to absorb longer wavelength in the visible light. This had been achieved by incorporating CuO onto TiO_2. The estimated band gap is shown in Table 5.1 in which it has been reduced from 3.2 eV to 2.9 eV. The lowered band gap reduction may be due to the presence of CuO crystals incorporated onto TiO_2. The study showed that the incorporation of transition metals tremendously improved the photocatalytic activity compared to TiO_2.

Furthermore, the preparations of the photocatalyst play an important role in the photocatalytic activity. Complex-precipitation and wet impregnation were the methods employed for comparisons. From the study carried out, the Cu/TiO_2 photocatalyst

prepared by complex-precipitaiton showed good photocatalytic performances compared to the wet impregnation. The highest amount obtained is 8.5 $mL^{-1}h^{-1}$ and 4.0 $mLg^{-1}h^{-1}$ for complex-precipitation and wet impregnation methods. The good performance is suggested to be contributed by the addition of glycerol as the most important intermediate complex ($Cu(C_3H_6O_3)$), which were formed through the reaction between Cu^{2+}, OH^- and glycerol. In this study, it is suggested that the dispersion degree of copper oxide species in the supports was very much depended on the copper loading, calcination temperature and method of preparation.

Table 5.1 Summary of the properties for the prepared photocatalyst.

Preparation methods	Photocatalyst	Surface area, m^2g^{-1}	Reduction temperature, °C	Band gap, eV	Photocatalytic reaction, $mLg^{-1}h^{-1}$
Complex precipitation	10CuGT3_30	42.20	251	2.9	8.5
	10CuGT4_30	45.13	264	2.9	6.8
	10CuGT5_30	42.38	285	2.75	5.7
Wet impregnation	10CuT3_30	63.83	233	2.4	4.0
	10CuT 4_30	42.69	172, 241	2.8	3.6
	10CuT 5_30	35.44	169, 241	2.5	2.7
	TiO_2	53.33	none	3.2	2.5

5.2 Recommendations

The findings in this study is very interesting and worth investigating. Further studies are recommended based on the current preparation methods in order to optimize the photocatalyst such as the aging time, pH, different precipitating agent and pretreatment (e.g: reduction after calcination). The improvement of the photocatalytic activity can be done by increasing the surface area of the photocatalyst by changing the calcinations conditions or preparation methods (e.g: by preparing smaller particles). It is recommended that more characterization need should be conducted for in-depth study of

the properties of the photocatalyst. Amongst the suggested analysis are XPS, AAS, TEM, TPD-H_2 and CO probing.

REFERENCES

Agus, H., Sandum, F., Naveen, M. and Sushil, A. (2005). "Current Status of Hydrogen Production Technique by Steam Reforming of Ethanol: A Review", *Energy and Fuels* 19: 2098-2106.

Akihiko, K. (2003). "Photocatalyst Materials for Water Splitting", *Catalysis Surveys from Asia* 7, 31-38.

Akihiko, K., Ryo, N., Akihide, I. and Hideki, K. (2007). "Effects of Doping of Metal Cations on Morphology, Activity and Visible Light Response of Photocatalysts", *Chemical Physics* 339, 104-110.

Akira, F. and Xintong, Z. (2006). "Titanium Dioxide Photocatalysis: Present Situation and Future Approches", *Comptes Rendus Chimie* 9: 750-760.

Albin, P., Jurka, B. and Stanko, H. (2005). "TPR, TPO and TPD Examinations of $CuO_{0.15}Ce_{0.85}O_{2-y}$ Mixed Oxides Prepared by Co-precipitation, by the Sol-gel Peroxide Route and by Citric Acid-assisted Synthesis", *Journal of Colloid and Interface Science* 285: 218-231.

Amit, S. and Sharma, B. P. (2002). "Preparation of Copper Powder by Glycerol Process", *Materials Research Bulletin* 37: 407-416.

Andrea, T., Ignazio, R. B., Vincenzo, B., Carmen, C., Massimiliano, D., Stefano, P., Roberto, S. and Franca, M. (2007). "Optimizing the Photocatalytic Properties of Hydrothermal TiO_2 by Control of Phase Composition and Particle Morphology. A Systematic Approach", *Journal of American Chemical Society* 129: 3564-3575.

Andrzej, S. (1991). "Hydrogen Photoproduction from Water-methanol on Titania Covered with Copper", *Monatsheft fur Chemie* 122: 645-652.

Ann, M. D., Robert, H. C. and Mark, R. O. (1998). "The Oxidative Chemistry of Methane over Supported Nickel Catalysts", *Catalysis Today* 46: 147-154.

Anna, G. and Jerzy, W. (2005). "Photocatalytic Water Splitting over Pt-TiO_2 in the Presence of Sacrificial Reagents", *Energy and Fuels* 19: 1143-1147.

Anpo, M. and Takeuchi, M. (2003). "The Design and Development of Highly Reactive Titanium Oxide Photocatalyst Operating under Visible Light Irradiation", *Journal of Catalysis* 216: 505-515.

Armor, J. N. (1999). "The Multiple Roles for Catalysis in The Production of H_2", *Applied Catalysis A: General* 176: 159-176.

Bak, T., Nowoty, J., Rekas, J. and Sorrell, C. C. (2002). "Photoelectrochemical Hydrogen Generation from Water Using Solar Energy: Materials Related Aspect", *International Journal of Hydrogen Energy* 27: 991-1022.

Bandara, J., Udawatta, C. P. K. and Rajapakse, C. S. K. (2005). "Highly Stable CuO Incorporated TiO_2 Catalyst for Photocatalytic Hydrogen Production from H_2O", *Journal of Photochemistry and Photobiological Science* 4: 857-861.

Behnajady, M. A., Modirshahla, N., Shokri, M. and Rad, B. (2008). "Enhancement of Photocatalytic Activity of TiO_2 Nanoparticles by Silver Doping: Photodeposition versus Liquid Impregnation Methods", *Global NEST Journal* 10: 1-7.

Binlin, D., Valerie, D., Paul, T. W., Haisheng, C. and Yulong, D. (2009). "Thermogravimetric Kinetics of Crude Glycerol", *Bioresource Technology* 100: 2613-2620.

Boccuzzi, F., Chiorino, A., Martra, G., Gargano, M., Ravasio, N. and Carrozzini, B. (1997). "Preparation, Characterization and Activity of Cu/TiO_2 Catalysts: Influence of

the Preparation Method on the Dispersion of Copper in Cu/TiO_2", *Journal of Catalysis* 165: 129-139.

Carl, A. and Allen, J. B. (1997). "Improved Photocatalytic Activity and Characterization of Mixed TiO_2/SiO_2 and TiO_2/Al_2O_3 Materials", *Journal of Physical Chemistry B* 101: 2611-2616.

Carp, O., Huisman, C.L., and Reller, A. (2004). "Photoinduced Reactivity of Titanium Dioxide," *Progress in Solid State Chemistry* 32: 33-117.

Chiang, K., Anal, R. and Tran, T. (2002). "Photocatalytic Degradation of Cyanide Using Titanium Dioxide Modified with Copper Oxide", *Advances in Environmental Research* 6: 471-485.

Colon, G., Maicu, M., Hidalgo, M. C. and Navio, J. A. (2006). "Cu-doped TiO_2 System with Improved Photocatalytic Activity", *Applied Catalysis B: Environmental* 67: 41-51.

Cordoba, G., Viniega, M., Fierro, J. L. G., Padilla, J. and Arroyo, R. (1998). "TPR, ESR and XPS Study of Cu^{2+} Ions in Sol Gel-derived TiO_2", *Journal of Solid State Chemistry* 138: 1-6.

Dana, D., Vlasta, B., Milan. and Mounir, A. M. (2002). "Investigation of Metal-doped Titanium Dioxide Photocatalysts", *Applied Catalysis B: Environmental* 37: 91-105.

Dhanalakshmi, K. B., Latha, S., Anandan, S. and Maruthamuthu, P. (2001). "Dye Sensitized Hydrogen Evolution from Water", *International Journal of Hydrogen Energy* 26: 669-674.

Diamandescu, L., Vasilia, F. and Tarabasanu, M. (2008). "Structural and Photocatalytic Properties of Iron and Europium-doped TiO_2 Nanoparticles Obtained under Hydrothermal Conditions", *Materials Chemistry and Physic* 112: 146-153.

Dong, H. K., Duck, K. C., Sun, J. K. and Kyung, S. L. (2008). "The Effect of Phase Type on Photocatalytic Activity in Transition Metal doped TiO_2 Nanoparticles", *Catalysis Comunications* 9: 654-657.

Dong, H. K., Ha, S. P., Sun, J. K. and Kyung, S. L. (2005). "Characteristic of Ni 8 wt%-doped Titanium Dioxide Photocatalyst Synthesized by Mechanical Alloying", Catalysis Letters 100: 49-52.

Dong, W. H., Hyung, G. K., Jum, S. J., Sang, W. B., Sang, M. J. and Jae, S. L. (2004). "Photocatalytic Decomposition of Water-methanol Solution Over Metal-doped Layered Pervoskite under Visible Light Irradiation", *Catalysis Today* 95: 845-850.

Dong, W. H., Jindo, K., Tae, J. P. and Jae, S. L. (2002). "Mg-doped WO_3 as a Novel Photocatalyst for Visible Light-induced Water Splitting", *Catalysis Letter* 80: 53-57.

Feg, W. C., Tyng, J. H. and Jui, D. S. (1998). "Hydrogenation of CO_2 Over a Rice Husk Ash Supported Nickel Catalyst Prepared by Deposition-Precipitation", *Industrial Engineering Chemical Resource* 37: 3838-3845.

Fuerte, A., Hernandez-Alonso, M. D., Maira, A. J., Martinez-Arias, A., Fernandez-Gracia, M., Conesa, J. C., Soria, J. and Munuera, G. (2002). "Nanosize Ti-W Mixed Oxides: Effect of Doping Level in the Photocatalytic Degradation of Toulene using Sunlight-type Excitation", *Journal of Catalysis* 212: 1-9.

Gen, T. Z., Qi, Z. Y., Xinchen, W. and Jimmy, C. Y. (2006). "Preparation and Characterization of Nanoplatelets of Nickel Hydroxides and Nickel Oxide", *Materials Chemistry and Physics* 98: 267-272.

Goncalves, G., Lenzi, M. K., Santos, O. A. A. and Jorge, L. M. M. (2006). "Preparation and Characterization of Nickel Based Catalysts on Silica, Alumina and Titania Obtained by Sol-gel Method", *Journal of Non-Crystalline Solids* 352: 3697-3704.

Gratian, B. R., Tsubota, S., Nakamura, T. and Haruta, M. (1995). "Photoassisted Hydrogen Production from Water-ethanol Solution: A Comparison of Activities of Au-TiO_2 and Pt-TiO_2", *Journal of Photochemistry and Photobiology A: Chemistry* 89: 177-189.

Gurunathan, K., Maruthamuthu, P. and Sastri, V. C. (1997). "Photocatalytic Hydrogen Production by Dye-sensitized Pt/SnO_2 and Pt/SnO_2/RuO_2 in Aqueous Methyl Viologen Solution", *International Journal of Hydrogen Energy* 22: 57-62.

Ha, S. P., Dong, H. K., Sun, J. K. and Kyung, S. L. (2006). "The Photocatalytic Activity of 2.5 wt% Cu-doped TiO_2 Nano Powders Synthesized by Mechanical Alloying", *Journal of Alloy and Compounds* 415: 51-55.

Haruhiko, T. and Tomoko, S. (1982). "The Simultaneous Determination of the Kinetics and Thermodynamics of $Cu(OH)_2$ Decomposition by Means of TG and DSC", *Thermochimica Acta* 54: 273-280.

Hedge, M. S., Larchen, D., Dupont, L., Beaudoin, B., Tekaia, K. E. and Jin, T. (1997). "Synthesis and Chemical Reactivity of Polyol Prepared Monodisperse Nickel Powders", *Solid State Ionics* 93: 35-50.

Heondo, J., Taehwan, K., Dongsik, K. and Kweoonill, K. (2006). "Hydrogen Production by the Photocatalytic Overall Water Splitting On NiO/$Sr_3Ti_2O_7$: Effect of Preparation", *International Journal of Hydrogen Energy* 31: 1142-1146.

Hideki, K. and Akihiko, K. (1999), "Highly Efficient Decomposition of Pure Water into H_2 and O_2 over $NaTaO_3$ Photocatalysts", *Catalysis Letters* 38: 153-155.

Hironori, A. and Kazuhiko, S. (2000). "Solar Hydrogen Production: Significant Effect of Na_2CO_3 Addition on Water Splitting using Oxide Semiconductor Photocatalysts", *Catalysis Survey from Japan* 4: 75-80.

Hyung, J. C. and Misook, K. (2007). "Hydrogen Production from Methanol/Water Decomposition in a Liquid Photosystem using The Anatase Structure of Cu Loaded TiO_2", *International Journal of Hydrogen Energy* 32: 3841-3848.

Jae, S. L. (2005). "Photocatalyst Water Splitting Under Visible Light with Particulate Semiconductors Catalyst", *Catalysis Surveys from Asia* 9, 217-228.

Jeevanandam, P., Mulukutla, R. S., Philips, M., Chaudhuri, S., Erison, L. E. and Klabunde, K. J. (2007). "Near Infrared Reflectance Properties of Metal Oxide Nanoparticles", *Journal of Physical Chemistry C* 111: 1912-1918.

Jeon, M. K., Jae, W. P. and Misook, K. (2007). "Hydrogen Production from Methanol/Water Decomposition in a Liquid Photosystem using The Anatase and Rutile Forms of Cu-TiO_2", *Journal of Industrial Engineering Chemistry* 13: 84-91.

Jin, Z., Xiaojie, Z., Yuexiang, L., Shuben, L. and Gongxuan, L. (2007). "5.1 % Apparent Quantum Efficiency for Stable Hydrogen Generation Over Eosin-sensitized CuO/TiO_2 Photocatalyst under Visible Light Irradiation", *Catalysis Communications* 8: 1267-1273.

Jing, D. and Guo, L. (2007). "WS_2 Sensitized Mesoporous TiO_2 for Efficient Photocatalytic Hydrogen Production from Water under Visible Light Irradiation", *Catalysis Communications* 8: 795-799.

Joachim, K., Gunter, S. E. and Nils, I. J. (1997). "UV-visible Diffuse Reflectance Spectroscopy of Zeolite-hosted Mononuclear Titanium Oxide Species", *Journal of Physical Chemistry B* 101: 1305-1311.

Jolanta, R. G., Ireneusz, S., Jacek, R. and Dominik, R. (2003). "Preparation, Characterization and Activity of Nickel Supported on Silica-titania", *Applied Catalysis A: General* 247: 193-206.

Junya, S., Nobuo, S., Yoko, Y., Kazuhiko, M., Tsuyoshi, T., Junko, N. K., Michikazu, H., Hisayoshi, K., Kazunari, D. and Yasunobu, I. (2005). "RuO_2-loaded β-Ge_3N_4 as a Non-oxide Photocatalyst for Overall Water Splitting", *Journal of American Chemical Society* 127: 4150-4151.

Kaifu, Z., Pu, J. and Qiangwang, C. (2006). "Ni Hollow Nanospheres: Preparation and Catalytic Activity", *Journal of Nanoparticles*: 1-7.

Kazuhiko, M. and Kazunari, D. (2007). "New Non-oxide Photocatalysts Design for Overall Water Splitting under visible Light", *Journal of Physical Chemistry* 111: 7851-7861.

Kenning, Y., Dong, J. K., Hun, S. C. and Huanzhen, L. (2003). "Dispersed Rod Like Nickel Powder Synthesized by Modified Polyol Process", *Materials Letters* 57: 3992-2997.

Kida, T., Guan, G. Q., Yamada, N., Ma, T., Kimura, K. and Yoshida, A. (2004). "Hydrogen Production from Sewage Sludge Solubilized in Hot-compressed Water using Photocatalyst under Light Irradiation", *International Journal of Hydrogen Energy* 29: 269-274.

Kirchernova, J., Herrera, M. L. C. and Guy, C. D. K. (2005). "Photocatalytic Oxidation of n-butanol under Flourescent Visible Light Lamp over Commercial TiO_2 (Hombicat UV 100 and Degussa P25)", *Applied Catalysis A: General* 282: 321-332.

Ko, Y. G. and Lee, W. Y. (2002). "Effect of Nickel-loading Method on The Water-splitting Activity of a Layered $NiO_x/Sr_4Ti_3O_{10}$ Photocatalyst", *Catalysis Letters* 83: 157-160.

Komova, O. V., Simakou, A. V. R., Kochubei, D. I., Odegova, G. V., Kriventsou, V. V., Paukshitis, E. A., Ushakov, V. A., Sazonova, N. N. and Nikoro, T. A. (2000).

"Investigation of The State of Copper in Supported Copper-titanium Oxide Catalysts" *Journal of Molecular Catalysis A: Chemical* 161: 191-204.

Lacey, A. A. and Peter, R. G. (2006). "Method to Improve Linearity of Diffuse Reflection Mid-Infrared Spectroscopy", *Analytical Chemistry* 78: 8165-8167.

Larsson, P. O., Arne, A., Reine, L. W. and Bon, S. (1996). "Combustion of CO and Toluene; Characterization of Copper Oxide Supported on Titania and Activity Comparisons with Supported Cobalt, Iron and Manganese Oxide", *Journal of Catalysis* 163: 279-293.

Lee, S. G., Lee, S. W. and Lee, H. I. (2001). "Photocatalytic of Hydrogen Production from Aqueous Solution Containing CN^- as a Hole Scavenger", *Applied Catalysis A: General* 207: 173-181.

Lei, G., Mingxia, X. and Haibo, F. (2006). "Preparation and Characterization of Silver and Indium Vanadate co-doped TiO_2 Thin Film as Visible-light-activated Photocatalyst", *Journal of Sol-gel Science Technology* 40: 65-73.

Leofanti, G., Padovan, M., Tozzola, G. and Venturelli, B. (1998). "Surface Area and Pore Texture of Catalysts", *Catalysis Today* 41: 202-219.

Li, D., Haneda, H., Hishita, S. and Ohashi, N. (2005). "Visible-light Driven Nitrogen-doped TiO_2 Photocatalysis: Effect of Nitrogen Precursors on Their Photocatalysis for Decomposition of Gas-phase Organic Pollutants", *Materials Science and Engineering B* 117: 67-75.

Li, Y. X., Lu, G. X. and Li, S. B. (2003). "Photocatalytic Production of Hydrogen in Single Component and Mixture Systems of Electron Donors and Monitoring Adsorption of Donors by In Situ Infrared Spectroscopy", *Chemosphere* 52: 843-850.

Li, Y., Mei, C., Jerry, R., Yide, X. and Wenjie, S. (2006). "Glycerol-mediated Synthesis of Ni and Ni/NiO Core-shell Nanoparticle", *Materials Letter* 60: 750-753.

Lin, H. Y., Yueh, F. C. and Yu, W. C. (2007). "Water Splitting on $NiO/InVO_4$ Under Visible Light Irradiation", *International Journal of Hydrogen Energy* 32: 86-92.

Linacero, R., Aguado-Serrano, J. and Rojas-Cervantes, M. L. (2006). "Preparation of Mesoporous TiO_2 by the Sol-gel Method assisted by Surfactants", *Journal of Materials Science* 41: 2457-2464.

Liu, L., Liejin, G., Wei, Y. and Hongtan, L. (2006). "A Composite Visible Light Photocatalysts for Hydrogen Production", *Journal of Power Source* 159: 13000-13004.

Livraghi, S., Votta, A., Cristina, P. and Giamello, E. (2005). "The Nature of Paramagnetic Species in Nitrogen Doped TiO_2 Active in Visible Light Photocatalysis", *Chemistry Communications*: 498-500.

Maeda, M. and Yamada, T. (2007). "Photocatalytic Activity of Metal-doped titanium Oxide Films Prepared by Sol-gel Process", *Journal of Physics: Conference Series* 61: 755-759.

Marc, H., Christian, B. and Jacques, L. (1996). "Synthesis and Characterization of Copper (II) Hydroxides Gels", *Journal of Sol-Gel Science and Technology* 6: 155-167.

Marta, C. N. A. C., Fabio, B. P. and Martin, S. (2002). "Quantification of Metallic Area of High Dispersed Copper on ZSM-5 Catalyst by TPD of H_2", *Catalysis Communications* 3: 503-509.

Masaaki, K., Masaya, M., Michio, U. and Masakazu, A. (2007). "Recent Developments in Titanium Oxide-based Photocatalysts", *Applied Catalysis A: General* 325: 1-14.

Masakazu, A. (1997). "Photocatalysis on Titanium Oxide Catalysts: Approaches in Achieving Highly Efficient Reactions and Realizing the Used of Visible Light", *Catalysis Surveys form Japan* 1: 169-179.

Masaya, M., Masaaki, K., Masato, T., Koichiro, T., Masakazu, A. and John, M. T. (2007). "Photocatalysis for New Energy Production: Recent Advances in Photocatalytic Water Splitting Reactions for Hydrogen Production", *Catalysis Today* 122: 51-56.

Meng, N., Micheal, K. H. L., Dennis, Y. C. L. and Sumathy, K. (2007). "A Review and Recent Developments in Photocatalytic Water-splitting using TiO_2 for Hydrogen Production", *Renewable and Sustainable Energy Reviews* 11: 401-425.

Meng, N., Micheal, K. H. L., Sumathy, K. and Dennis, Y. C. L. (2006). "Potential of Renewable Hydrogen Production for Energy Supply in Hong Kong", *International Journal of Hydrogen Energy* 31: 1401-1412.

Mile, B., Stirling, D. and Zammit, M. A. (1990). "TPR Studies of the Effects of Preparation Conditions on Suported Nickel Catalysts", *Journal of Molecular Catalysis* 62: 179-198.

Min, K. J., Jae, W. P. and Misook, K. (2007). "Hydrogen Production from Methanol/Water Decomposition in a Liquid Photosystem Using the Anatase and Rutile Forms of Cu-TiO_2", *Journal of Industrial Engineering Chemistry* 13: 84-91.

Momirlan, M. and Veziroglu, T. (1999). "Recent Direction of World Hydrogen Production", *Renewable and Sustainable Energy Reviews* 3, 219-231.

Moura, J. A., Araujo, A. S., Ana, C. S. L. S. C., Joana, M. F. B. A., Silva, A. O. S. and Souza, M. J. B. (2005). "Thermal Analysis Applied to Characterization of Copper and Nickel Catalysts", *Journal of Thermal Analysis and Calorimetry* 79: 435-438.

Murphy, A. B. (2007). "Band Gap Determination from Diffuse Reflectance Measurement of Semiconductor Films and Application to Photoelectrochemical Water Splitting", *Solar Energy Materials and Solar Cell* 91: 1326-1337.

Nada, A. A., Barakat, M. H., Hamed, H. A., Mohamed, N. R. and Veziroglu, T. N. (2005). "Studies on The Photocatalytic Hydrogen Production using Suspended Modified TiO_2 Photocatalysts", *International Journal of Hydrogen Energy* 30: 687- 691.

Nakamoto, K. (1997). "*Infrared and Raman Spectra of Inorganic and Coordination Compounds. Part B: Application in Coordination, Organometallic and Bioinorganic Chemistry*", 5th ed., John Wiley & Sons, USA.

Niu, H., Qing, Y. and Kaibin, T. (2006). "A New Route to Copper Nitrate Hydroxide Microcrystal", *Materials Science and Engineering B* 135: 172-175.

Nowotny, J., Sorrell, C. C., Bak, T. and Sheppard, L. R. (2005). "Solar-hydrogen: Unresolved Problems in Solid-state Science", *Solar Energy* 78: 593-602.

Paola, A. D., Ikeda, S., Marci, G., Bohtani, B. and Palmisano, L. (2001). "Transition Metal Doped TiO_2: Physical Properties and Photocatalytic Behaviour", *International Journal of Photoenergy* 3: 171-176.

Park, M. and Kang, M. (2008). "The Preparation of Anatase and Rutile Forms of Ag-TiO_2 and Hydrogen Production from Methanol/water Decomposition", Materials Letters 62: 183-187.

Porkodi, K. and Arokiamary, S. D. (2007). "Synthesis and Spectroscopic Characterization of Nanostructured anatase Titania: A Photocatalyst", *Materials Characterization* 58: 495-503.

Premkumar, J. (2004). "Development of Super-hydrophilicity on Nitrogen-doped TiO_2 Thin Film Surface by Photoelectrochemical Method under Visible Light", *Chemistry Materials* 16: 3980-3981.

Rahimnejad, S., Rahman, S. S. and Gholami, M. R. (2008). "A Credible Role of Copper Oxide on Structure of Nanocrystalline Mesoporous Titanium Dioxide", *Journal of Iranian Chemical Society* 5: 367-374.

Sadhana, S. R., Nidhi, D., Nitin, K. L., Kagne, S. and Sukumar, D. (2007). "UV and Visible Active Photocatalysts for Water Splitting Reaction", *International Journal of Hydrogen Energy* 32: 2776-2783.

Sakthivel, S., Hidalgo, M. C., Bahnemann, S. U. G., Murugesan, D. W. and Vegelpohl, A. (2006). "A Fine Route to Tune the Photocatalyst Activity of TiO_2", *Applied Catalysis B: Environmental* 63: 31-40.

Sakthivel, S., Shankar, M. V., Palanichamy, M., Arabindoo, B., Bahnemann, D. W. and Murugesan, V. (2004). "Enhancement of Photocatalytic Activity By Metal Deposition: Characterization and Photonic Efficiency of Pt, Au and Pd Deposited On TiO_2 Catalyst", *Water Resource* 38: 3001-3008.

Sayama, K. and Arakawa, H. (1996). "Effect of Carbonate Addition on the Photocatalytic Decomposition of Liquid Water over ZrO_2 Catalyst", Journal of Photochemical and Photobiological A: Chemistry 94: 67-76.

Sayama, K., Arakawa, H. and Domen, K. (1996). "Photocatalytic Water Splitting on Nickel Intercalated", *Catalysis Today* 28: 175-182.

Sayama, K., Tanaka, A., Domen, K., Maruya, K. and Onishi, T. (1990). "Improvement of Nickel-loaded $K_4Nb_6O_{17}$ Photocatalyst for The Decomposition of H_2O", *Catalysis Letters* 4: 217-222.

Senevirathna, M. K. I., Pitigala, P. K. D. D. P. and Tennakone, K. (2005). "Water reduction with Cu_2O Quantum Dots on TiO_2 Nano-particles", *Journal of Photochemistry and Photobiology A: Chemistry* 171: 257-259.

Shi, D., Yaqing, F. and Shunhe, Z. (2004). "Photocatalytic Conversion of CH_4 and CO_2 to Oxygenated Compound over Cu/CdS-TiO_2/SiO_2 Catalyst", *Journal of Catalyst Today* 98, 505-509.

Singto, S., Sarapong, P., Yoshikazu, S. and Susumu, Y. (2005). "Photocatalytic Activity of Titania Nanocrystals Prepared by Surfactant-assisted Templating Method-effect of Calcination Conditions", *Materials Letters* 59: 2956-2968.

Slamet, H. W.N., Ezza, P., Soleha, K. and Jarnuzi, G. (2005). "Photocatalytic Reduction of CO_2 On Copper-doped Titania Catalysts Prepared by Improved-impregnation Method", *Catalysis Communications* 6: 313-319.

Suda, Y., Kawasaki, H., Ueda, T. and Ohshima, T. (2004). "Preparations of High Quality Nitrogen doped TiO_2 Thin Film as a Photocatalyst using a Pulsed Laser Deposition Method", *Thin Film Solid* 453-454: 162-166.

Sun, H., Wang, H. and Zhang, J. (2006). "Preparation and Characterization of Nickel-titanium Composite Xerogel Catalyst for CO_2 reforming of CH_4", Applied Catalysis B: Environmental *(Article in Press)*

Sun, J., Yan, J., Yong, Z. J., Monique, T. and Claude, B. (2005). "Mechanism of Preparing Ultrafine Copper Powder by Polyol Process", *Materials Letters* 59: 3933-3936.

Teruhisa, O., Koji, S., Kojiro, T. and Michio, M. (2001). "Morphology of a TiO_2 Photocatalyst (Degussa, P-25) Consisting of Anatase and Rutile Crystalline Phases", *Journal of Catalysis* 203: 82-86.

Thammanoon, S., Yoshikazu, S. and Susumu Y. (2005). "Photocatalytic Evolution of Hydrogen over Mesoporous TiO_2 Supported NiO Photocatalyst Prepared by Single-step Sol-gel Process with Surfactant Template", *International Journal of Hydrogen Energy* 30: 1053-1062.

Tseng, I. H. and Wu, J. C. S. (2004). "Chemical States of Metal-loaded Titania in the Photoreduction of CO_2", *Catalysis Today* 97: 113-119.

Tseng, I. H., Wan, C. C. and Wu, J. C. S. (2002). "Photoreduction of CO_2 using Sol-gel Derived Titania and Titania-supported Copper Catalysis", *Applied Catalysis B: Environmental* 37: 37-48.

Valdeilson, S. D., Fillipe, A. C. G., Jose, A. D. and Silva, C. L. D. (2007). "Copper Oxide and Niobium Pentoxide Supported on Silica-alumina: Synthesis, Characterization and Application on Diesel Soot Oxidation", *Journal of Catalysis* 247: 68-77.

Wilke, K, and Breuer, H. D. (1999). "The Influence of Transition Metal Doping on The Physical and Photocatalytic Properties of Titania," *Journal of Photochemistry and Photobiology A: Chemistry* 121: 49-53.

Wu, J. C. S. and Chih, Y. Y. (2001). "Sol-gel-derived Photosensitive TiO_2 and Cu/TiO_2 Using Homogeneous Hydrolysis Technique", *Journal of Materials Resources* 16: 615-620.

Wu, N. L. and Lee, M. S. (2004). "Enhanced TiO_2 Photocatalysis by Cu in Hydrogen Production from Aqueous Methanol Solution", *International Journal of Hydrogen Energy* 29: 269-274.

Wu, T., Qiangu, Y. and Hiulin, W. (2005). "Partial Oxidation of Methane to Hydrogen and Carbon Monoxide over a Ni/TiO_2 Catalyst", *Journal of Molecular Catalysis* A: Chemical 226: 41-48.

Xin, B., Peng, W., Dandan, D., Jia, L., Zhiyu, R. and Honggang, F. (2008). "Effect of Surface Species on Cu/TiO_2 Photocatalytic Activity", *Applied Surface Science* 254: 2569-2574.

Xu, J. C., Shi, Y. L., Huang, J. E., Wang, B. and Li, H. L. (2004). "Doping Metal Ions only onto the Catalyst Surface," *Journal of Molecular Catalysis A: Chemical* 219: 351-355.

Yan, X., He, J., Evans, D. G., Zhu, Y. and Duan, X. (2004). "Preparation, Characterization and Photocatalytic Activity of TiO_2 Formed from a Mesoporous Precursor", *Journal of Porous Materials* 11: 131-139.

Yasomanee, J. P. and Bandara, J. (2008). "Multi Electron Storage of Photoenergy using Cu_2O-TiO_2 Thin Film Photocatalyst", *Solar Energy Materials and Solar Cells* 92: 348-352.

Ye, J., Zou, Z. and Akiyuki, M. (2003). "A Novel Series of Water Splitting Photocatalysts NiM_2O_6 (M= Nb, Ta) Active Under Visible Light", *International Journal of Hydrogen Energy* 28: 651-665.

Yi, H., Peng, T., Ke, D., Ke, D., Zan, L. and Yan, C. (2008). "Photocatalytic H_2 Production from Methanol Aqueous Solution over Titania Nanoparticles with Mesostructures", *International Journal of Hydrogen Energy* 33: 672-678.

Yong, L., Mei, C., Jerry, R., Yide, X. and Wenjie, S. (2006). "Glycerol-mediated Synthesis of Ni and Ni/NiO Core-shell Nanoparticles", *Materials Letters* 60: 750-755.

Yuan, Z., Wang, Y., Sun., Y., Wang, J. and Bie, L. (2006). "Sunlight-activated $AlFeO_3/TiO_2$ Photocatalyst", *Science in China: Series B Chemistry* 49: 67-74.

Zaghib, K., Mauger, A., Goodenough, J. B., Gendron, F. and Julien, C. M. (2007). "Electronic, Optical and Magnetic Properties of $LiFePO_4$: Small Magnetic Polaron Effects", *Chemistry Materials* 19: 3740-3747.

Zhou, G. T., Qi, Z. Y., Xinchen, W. and Jimmy, C. Y. (2006). "Preparation and Characterization of Nanoplatelets of Nickel Hydroxide and Nickel Oxide", *Materials Chemistry and Physic* 98: 267-272.

Zhu, H., Yong, W., Xi, Z., Haiqin, W., Lijuan, Y., Jianming, H., Qing, Y., Lin, D., Yi, C., Can, J., Jun, W. and Penghui, X. (2006). "Influence of Impregnation Times on the Dispersion of CuO on Anatase", *Journal of Molecular Catalysis A: Chemical* 243: 24-30.

Zou, Z. and Arakawa, H. (2003). "Direct Water Splitting into H_2 and O_2 under Visible Light Irradiation with a New Series of Mixed Oxides Semiconductors Photocatalysts", *Journal of Photochemistry and Photobiology A: Chemistry* 158: 145-162.

Zou, Z., Jinhua, Y. and Hironori, A. (2002). "Surface characterization of Nanoparticles of $Ni/In_{0.9}NiO_{0.1}TaO_4$: Effects on Photocatalytic Activity", *Journal of Physical Chemistry B* 106: 13098-13101.

APPENDIX A

[CALCULATION FOR 0.25 M NaOH]

M.W. for NaOH : 40

$$\text{Numbers of mol} = \frac{\text{mass(g)}}{\text{M.W}} \quad (1)$$

$$\text{Molarity} = \frac{\text{mol}}{\text{volume(L)}} \quad (2)$$

Substitute eqn (1) into eqn (2),

$$\text{Molarity} = \frac{\frac{\text{mass(g)}}{\text{M.W}}}{\text{volume(L)}}$$

$$0.25 = \frac{\frac{\text{mass(g)}}{40}}{1\text{L}}$$

Therefore,

Mass of NaOH = **10 g**

APPENDIX B

[CALCULATION FOR Cu LOADING ON TiO_2]

	Metal loading, wt%					
	2	5	9	10	11	15
Mass of $Cu(NO_3)_2.3H_2O$, g	0.7615	1.9039	3.4269	3.8077	4.1885	5.7112
Mass of TiO_2, g	9.8	9.5	9.1	9	9.79	8.5

Example of calculation for 10wt% copper loading:-

To prepare, 100 g of catalyst 10 g of metals were needed. Therefore, to prepare 10 g of catalyst, 1g of metal was needed.

100 g of catalyst ⟶ 10 g of metals
10 g of catalyst ⟶ 1 g of metals

1 mol of $Cu(NO_3)_2.3H_2O$ ⟶ 63.546 g of Cu

x mol of $Cu(NO_3)_2.3H_2O$ ⟶ 1 g of Cu

$$\therefore x = \frac{1}{63.546} \times 1$$

$$= 0.01576 \text{ mol}$$

1 mol of $Cu(NO_3)_2.3H_2O$ ⟶ 241.60 g

0.01576 mol of $Cu(NO_3)_2.3H_2O$ ⟶ y g

$\therefore$ y = **3.8077 g (10wt%Cu)**

Mass of TiO_2 = 9 g

APPENDIX C

[EDX ANALYSIS]

a) 10CuT3_30

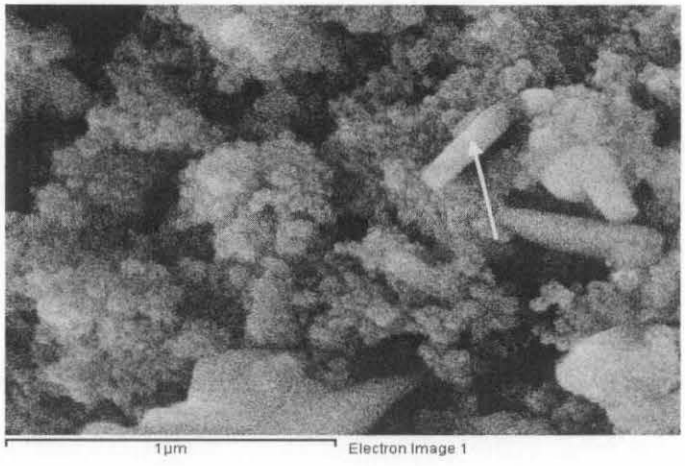

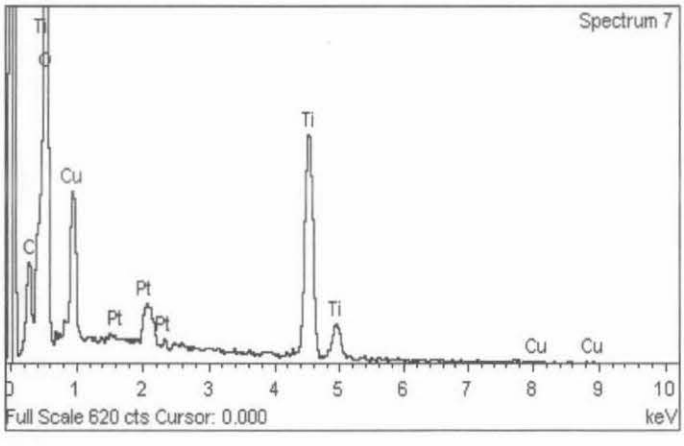

APPENDIX D

[BET RESULTS]

a) Adsorption-desorption Isotherm for TiO_2

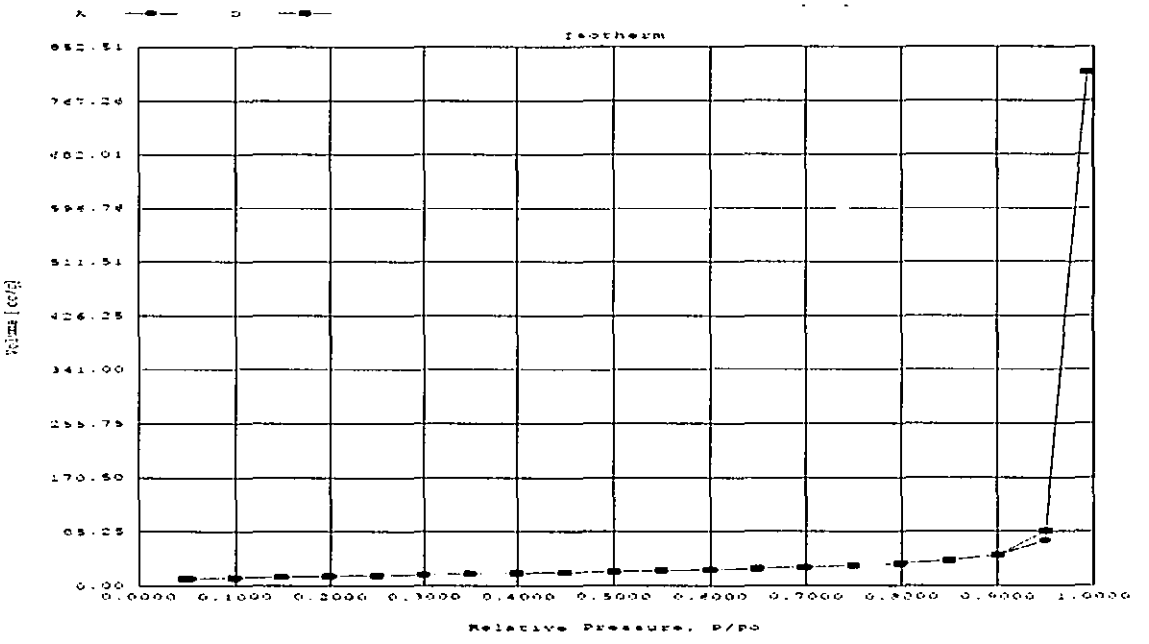

b) Adsorption-desorption Isotherm for 10CuGT3_30

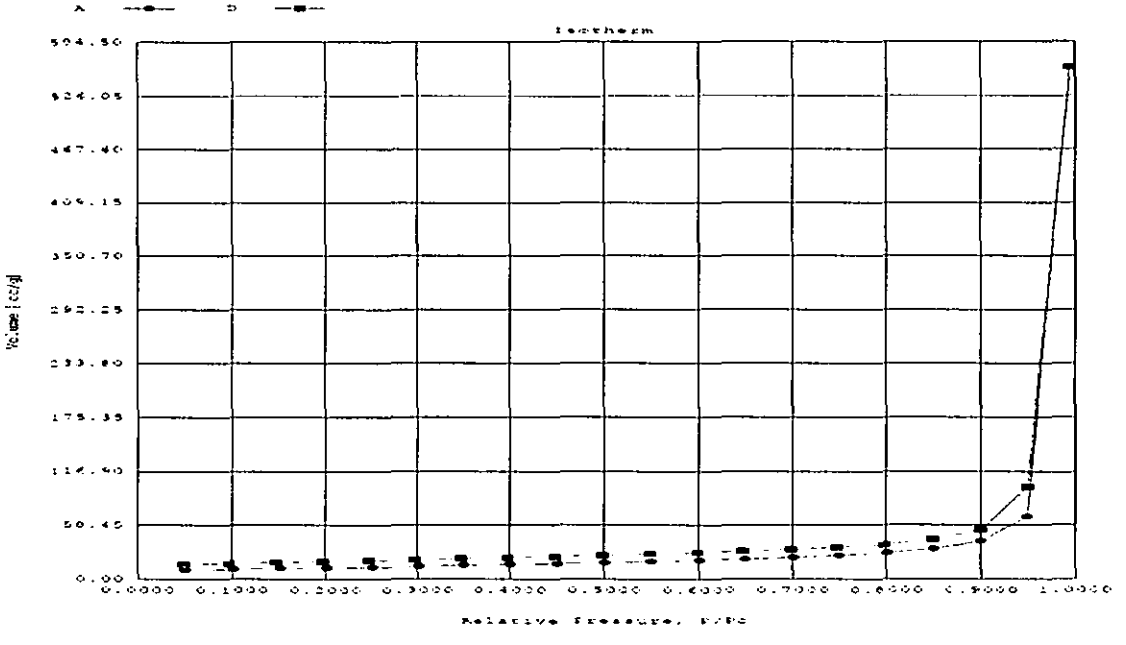

c) Adsorption-desorption Isotherm for 10CuGT4_30

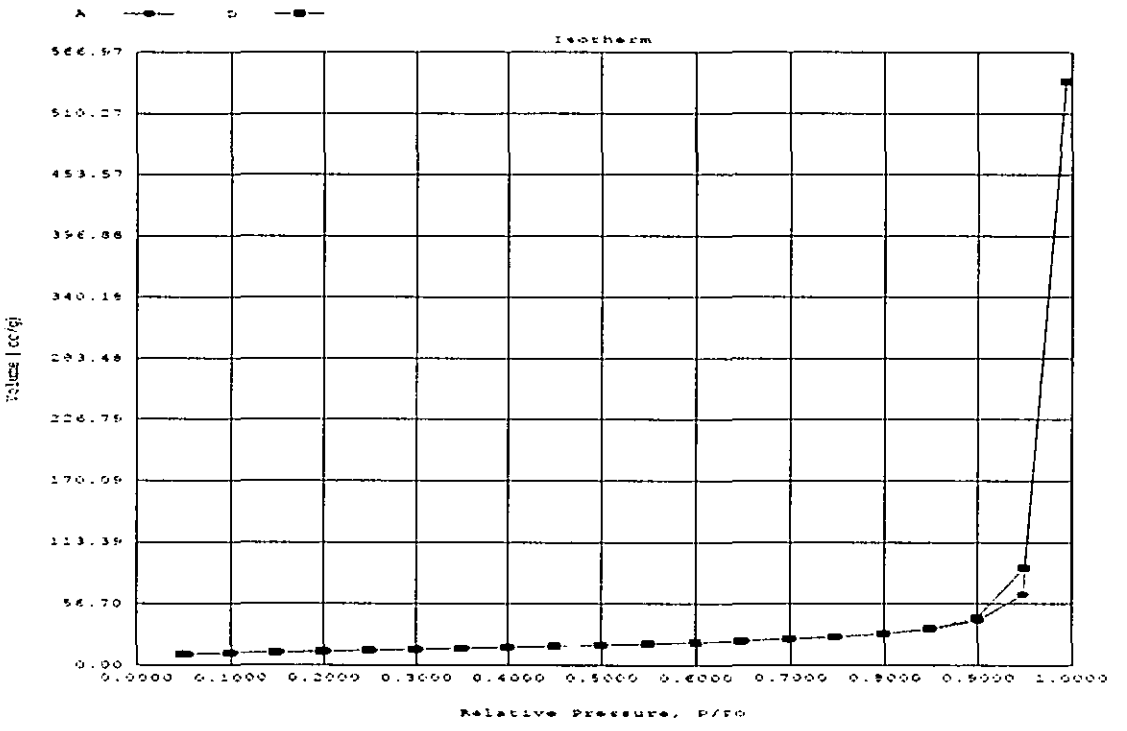

d) Adsorption-desorption Isotherm for 10CuGT5_30

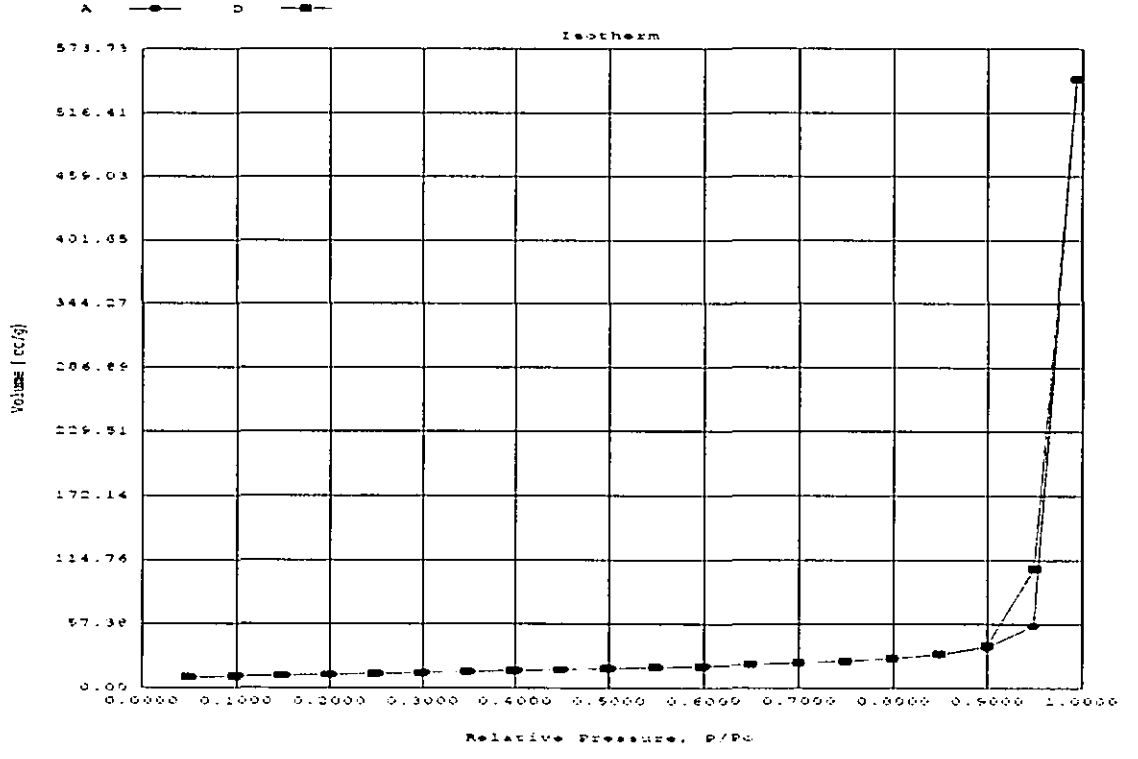

e) Adsorption-desorption Isotherm for 10CuT3_30

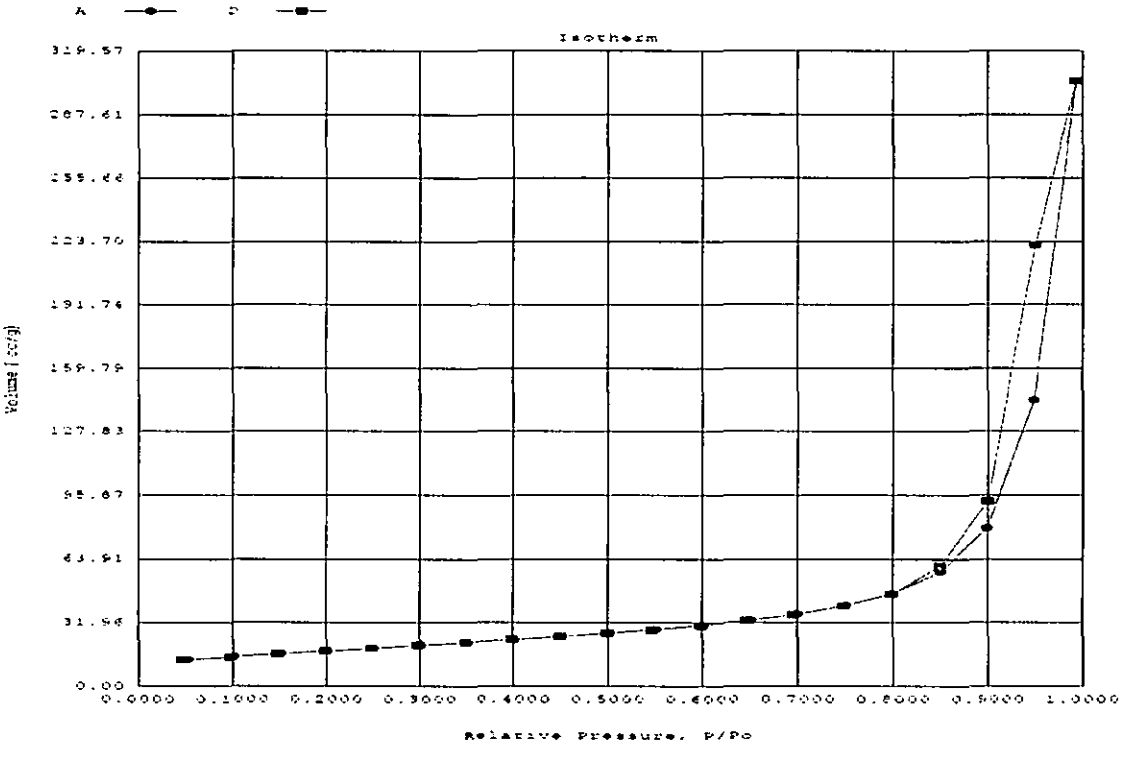

f) Adsorption-desorption Isotherm for 10CuT4_30

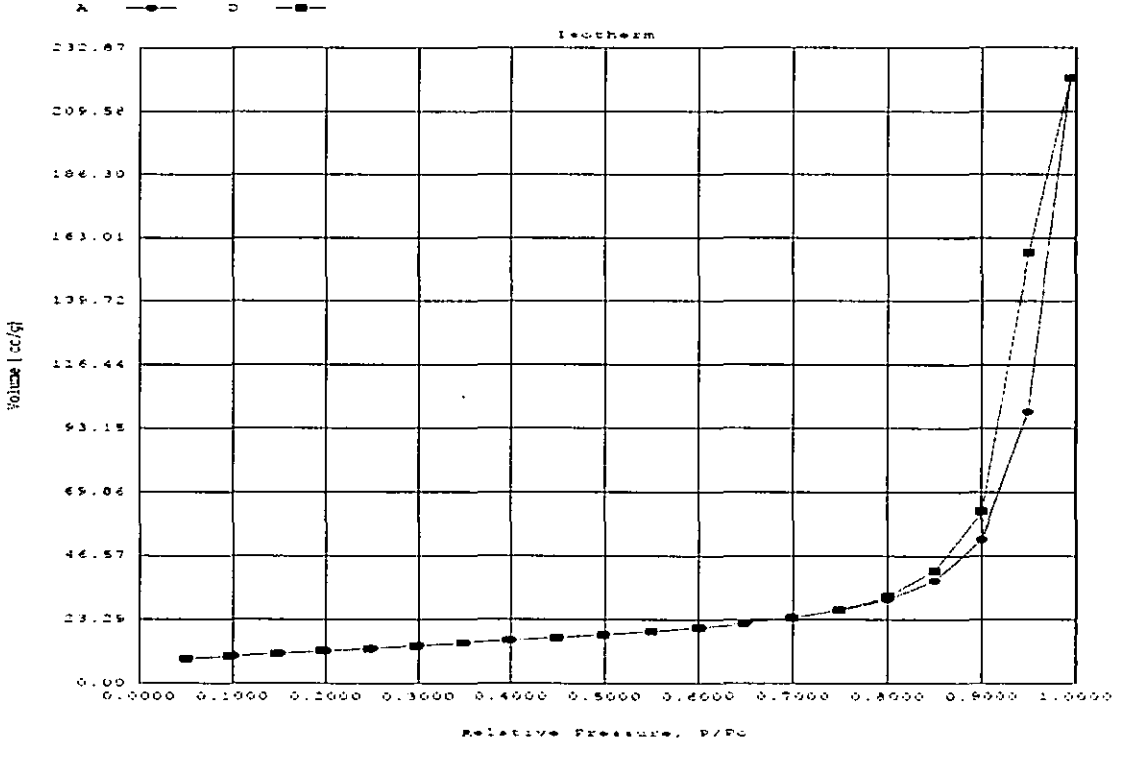

g) Adsorption-desorption Isotherm for 10CuT5_30

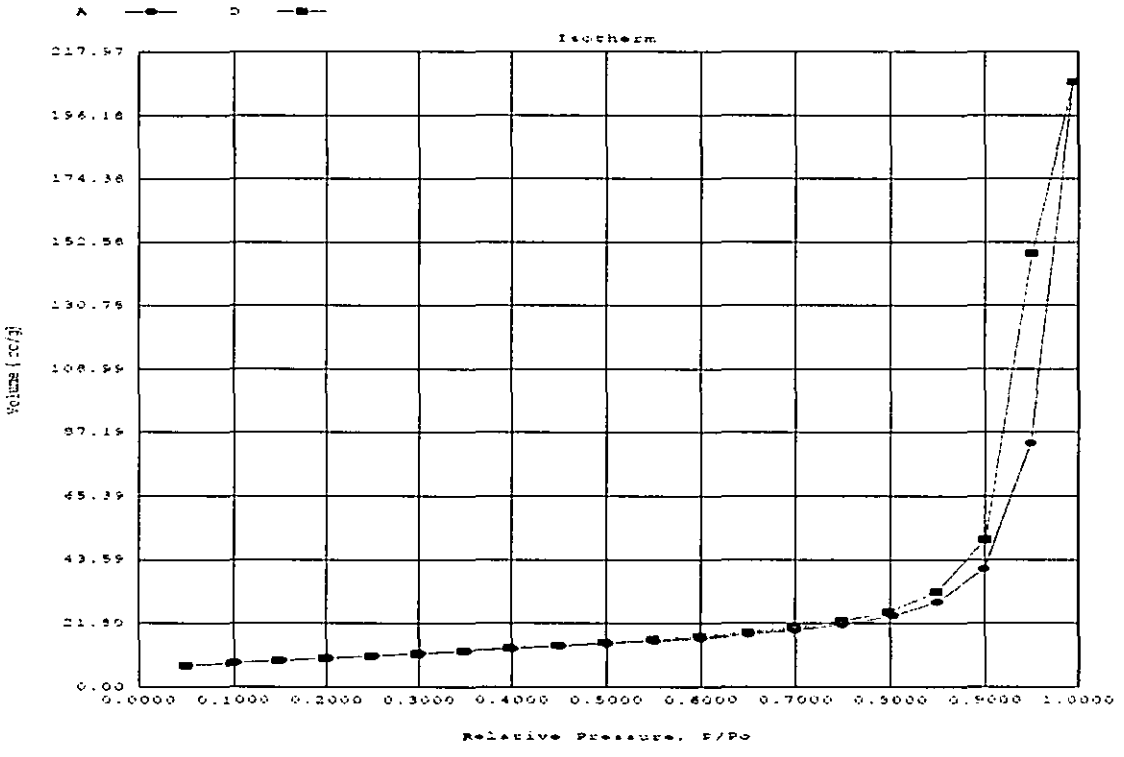

APPENDIX E

[XRD SPECTRA RESULTS]

a) XRD spectra for TiO_2

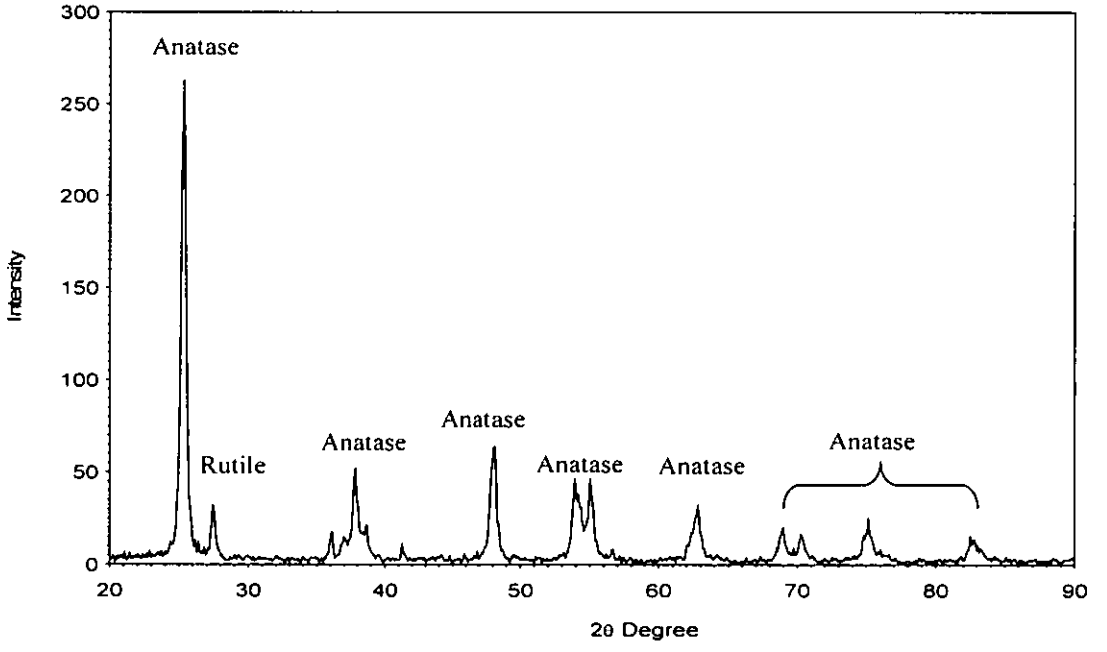

b) XRD spectra for 10CuGT3_30

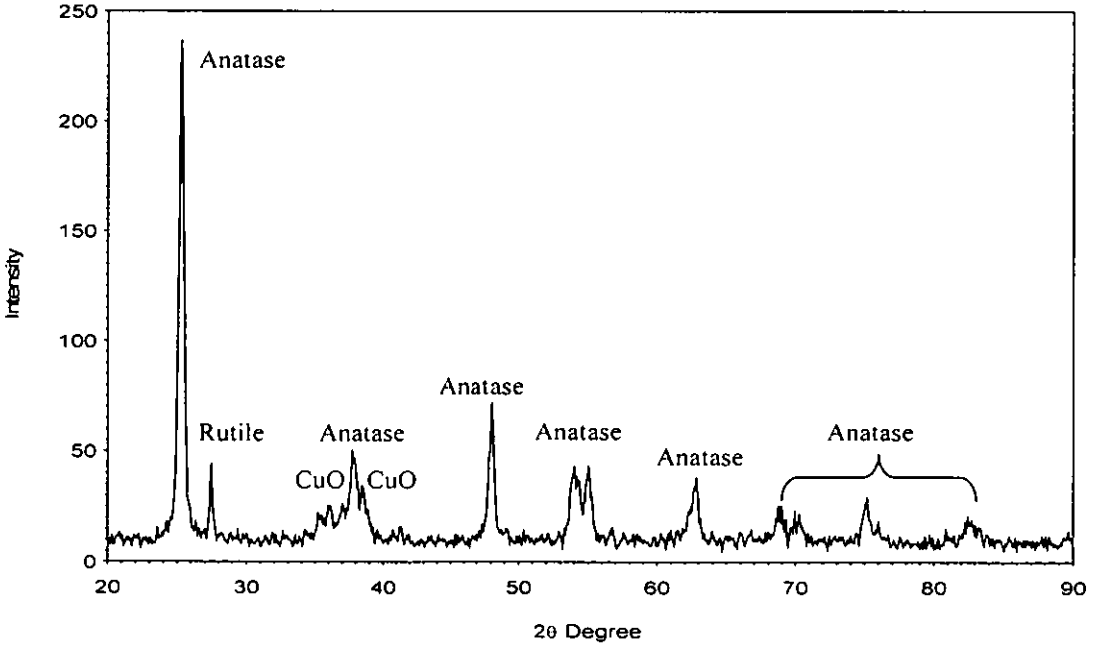

c) XRD spectra for 10CuGT4_30

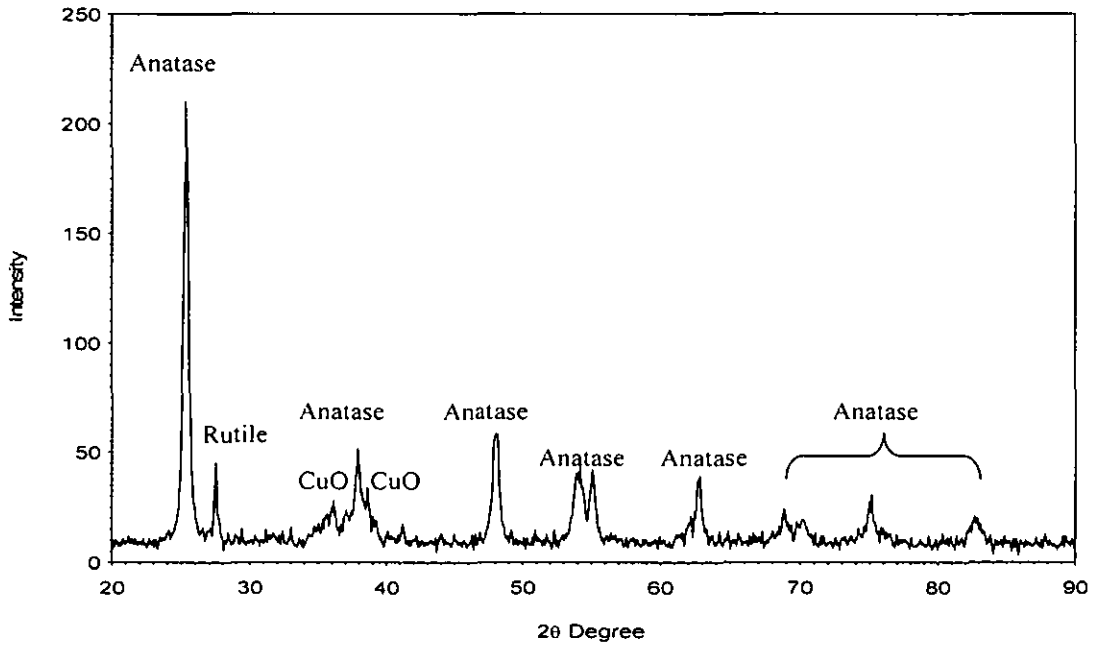

d) XRD spectra for 10CuGT5_30

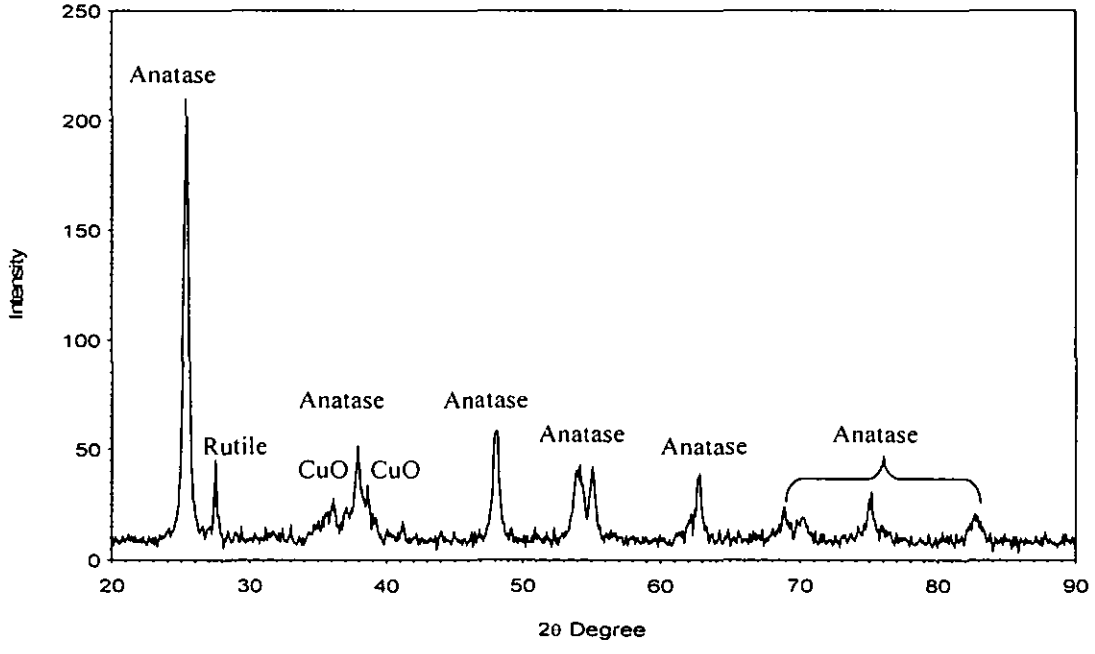

e) XRD spectra for 10CuT3_30

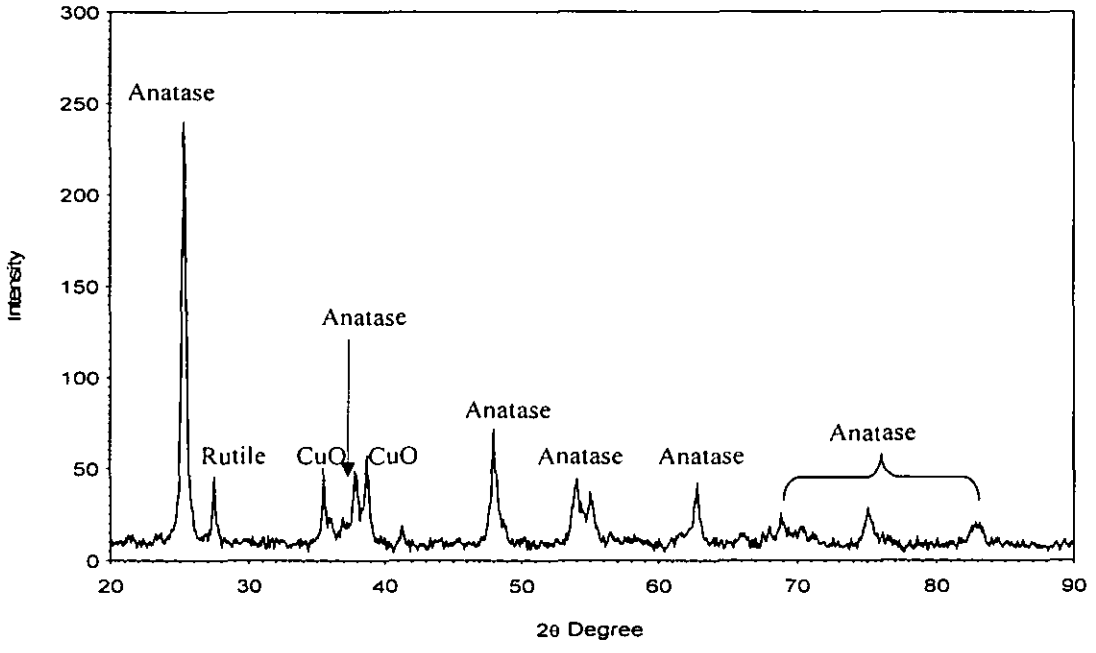

f) XRD spectra for 10CuT4_30

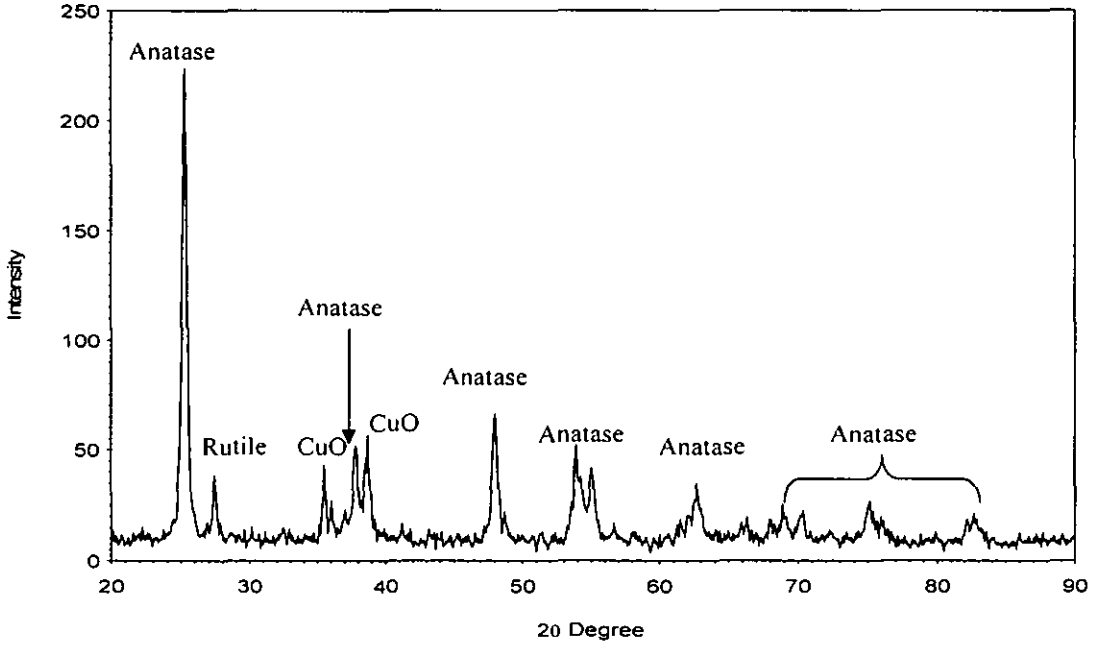

g) XRD spectra for 10CuT5_30

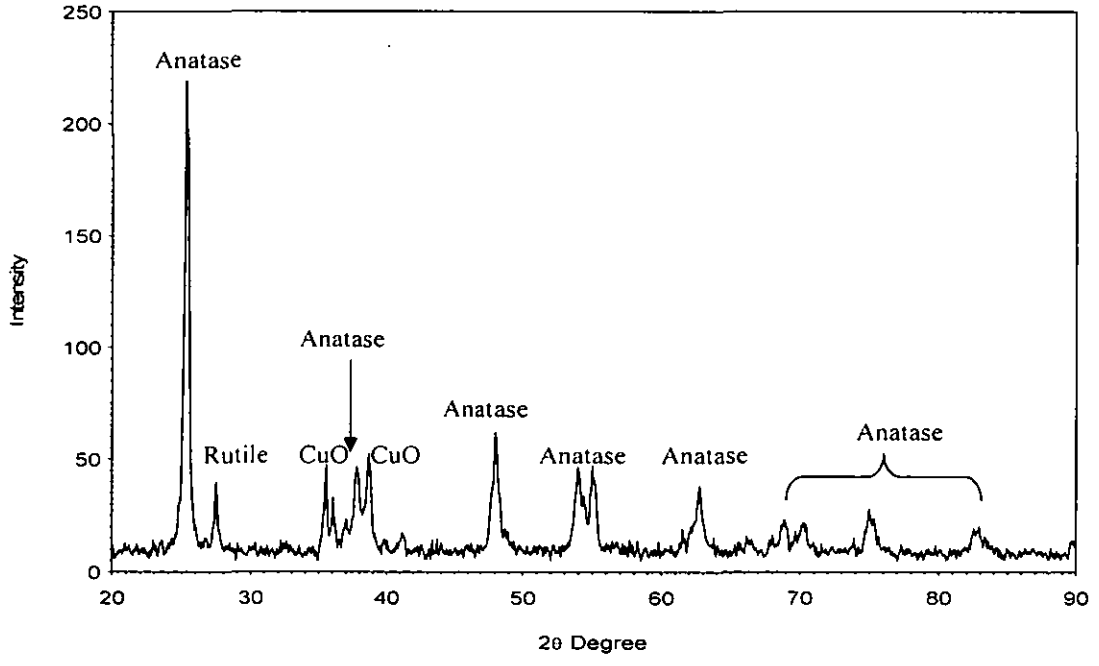

APPENDIX F

[BAND GAP ESTIMATION FROM DR-UV-VIS SPECTRA RESULTS]

a) The DR-UV-Vis spectra for TiO_2

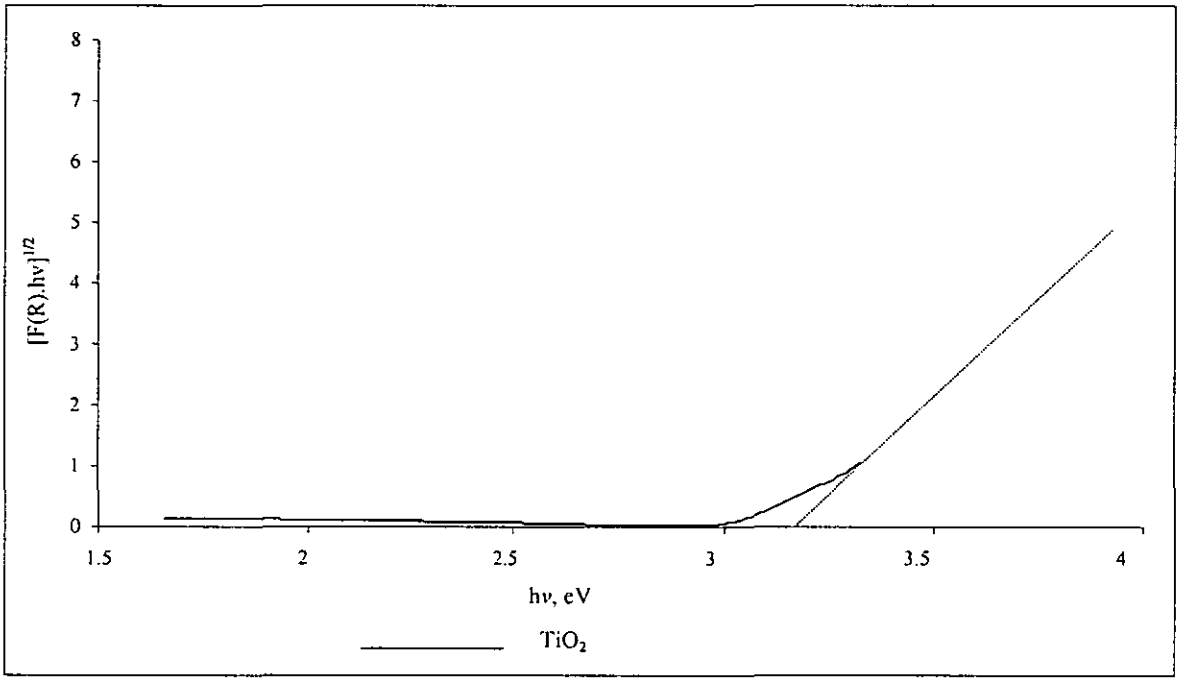

The band gap for TiO_2 is determined from the extrapolation of the absorption edge onto the energy axis (E_g) using the linear equation, $y = mx + c$.

Two plots were obtained from the linear curve of TiO_2: - (3.79412, 3.58661) and (3.45593, 1.54351)

$$m = \frac{(3.58661 - 1.54351)}{(3.79412 - 3.45593)}$$

$= 6.041278$

Insert (3.45593, 1.54351) into $y = mx + c$

$1.54351 = 6.4308(3.45593) + c$

Therefore, $c = -19.33472$

$y = 6.4308x - 19.33472$

When $y = 0$, $x = 3.20$

Therefore the estimated band gap for TiO_2 is 3.2 eV

APPENDIX G

[FTIR SPECTRA RESULTS]

a) FTIR spectra of glycerol

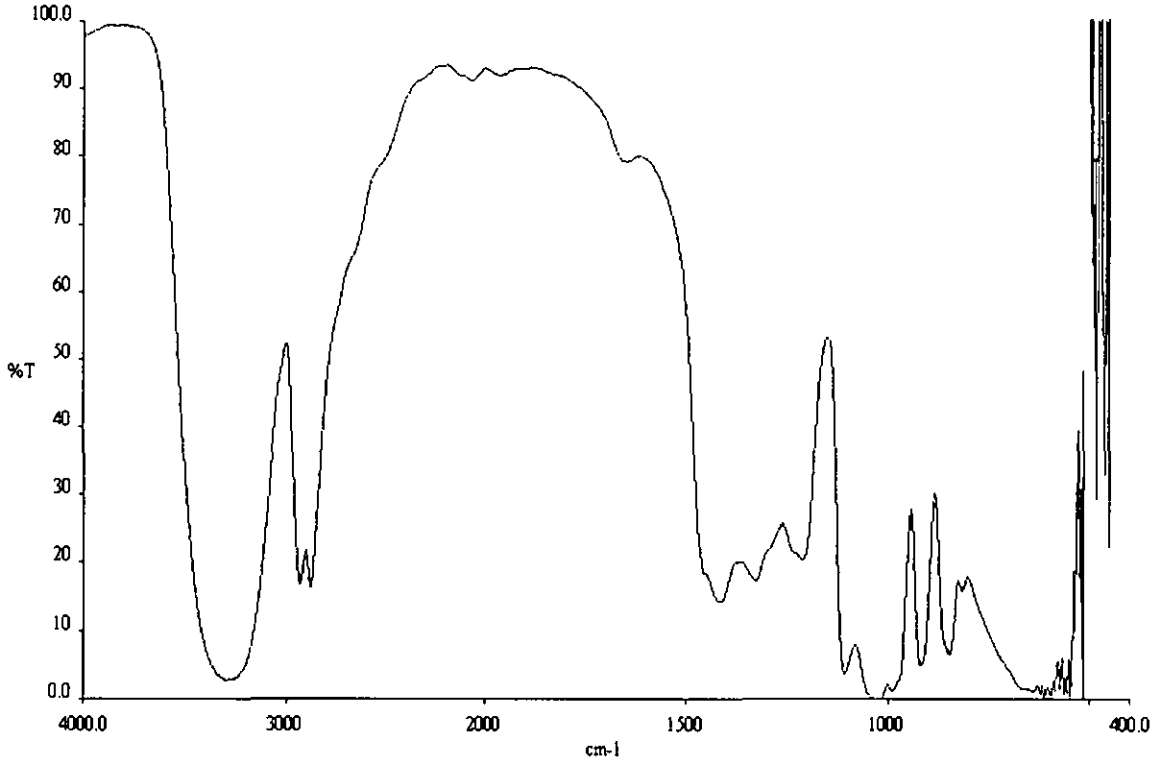

b) FTIR spectra of TiO_2

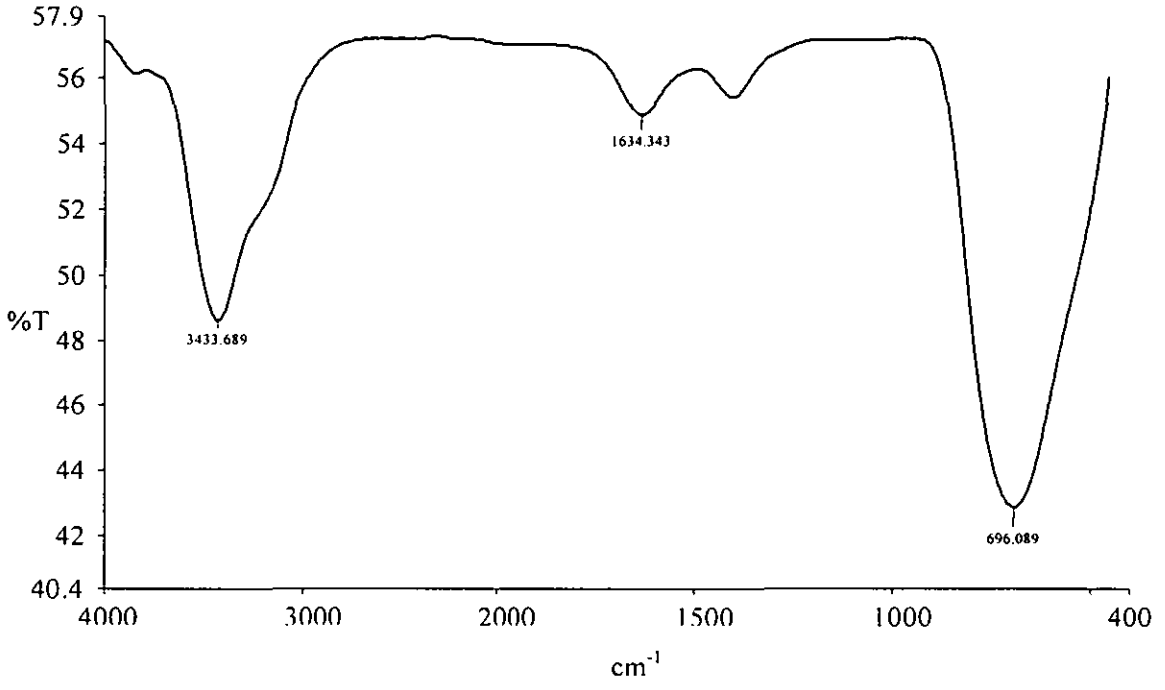

c) FTIR spectra of fresh Cu/TiO_2 prepared by complex-precipitation method

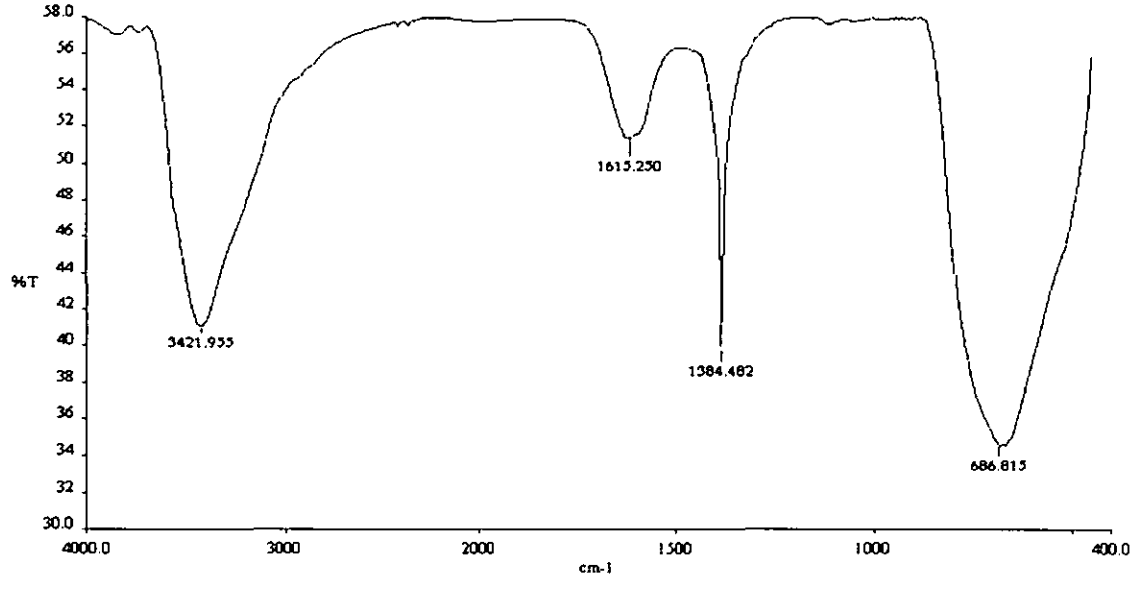

d) FTIR spectra of fresh Cu/TiO_2 prepared by wet impregnation method